The object of this study is the accuracy of aircraft positioning for open and covert video surveillance by an infocommunication network of optical-electronic stations along the trajectories of their movement. The task addressed is numerical assessment of the accuracy of aircraft positioning in airspace. It is proposed to use a convex polyhedron as a universal assessment of the accuracy of aircraft positioning, in which, with a given probability, the aircraft is located. It is shown that the lower estimate of this probability depends on the a priori information on the statistical properties of the errors in the estimates of the coordinates of the aircraft location, and the scattering ellipsoid, which is currently the main form of assessing the accuracy of aircraft positioning in airspace, is a special case and is always located inside a convex polyhedron.

The results reported here include the following:

– simulation models of open and covert video surveillance by an infocommunication network of optoelectronic stations along the trajectories of aircraft movement;

– a numerical method for estimating the uncertainty region in the form of a convex polyhedron, in which, with a given probability, the aircraft is located;

– dependence of change in the shapes and boundaries of the convex polyhedron on the errors of video surveillance and the mutual spatial location of the aircraft and the network of optoelectronic stations;

– software implementation of methods for constructing and visualizing the shapes and boundaries of uncertainty regions in the form of convex polyhedrons and scattering ellipsoids.

It is shown that the aircraft is inside the convex polyhedron with the probability $P \geq 0.8889$ for any distribution, $P \geq 0.9506$ for a symmetric one and $P \geq 0.9973$ for a normal distribution

Keywords: optoelectronic station, infocommunication network, aircraft, convex polyhedron, scattering ellipsoid

UDC 621.389
DOI: 10.15587/1729-4061.2025.330922

DEVISING A NUMERICAL METHOD FOR ESTIMATING THE POSITIONING ACCURACY OF AIRCRAFT BY AN INFORMATION-COMMUNICATION NETWORK OF OPTOELECTRONIC STATIONS

Andriy Tevyashev
Doctor of Technical Sciences, Professor*
Oleksii Haluza
Doctor of Physical and Mathematical Sciences, Professor
Department of Computer Mathematics and Data Analysis
National Technical University «Kharkiv Polytechnic Institute»
Kyrpychova str., 2, Kharkiv, Ukraine, 61002
Department of Software Engineering**
Dmytro Kostaryev
Doctor of Technical Sciences*
Anton Paramonov
PhD Student
Department of Information Technology Security**
Nataliia Sizova
Corresponding author
Doctor of Physical and Mathematical Sciences, Professor
Department of Applied Mathematics and Information Technology
O.M. Beketov National University of Urban Economy in Kharkiv
Chornoglazivska str., 17, Kharkiv, Ukraine, 61002
E-mail: sizova@ukr.net
*Department of Applied Mathematics**
**Kharkiv National University of Radio Electronics
Nauky ave., 14, Kharkiv, Ukraine, 61166

Received 14.03.2025
Received in revised form 25.04.2025
Accepted date 19.05.2025
Published date 25.06.2025

How to Cite: *Tevjashev, A., Haluza, O., Kostaryev, D., Paramonov, A., Sizova, N. (2025). Devising a numerical method for estimating the positioning accuracy of aircraft by an information- communication network of optoelectronic stations. Eastern-European Journal of Enterprise Technologies, 3 (9 (135)), 101–120. https://doi.org/10.15587/1729-4061.2025.330922*

1. Introduction

The task to improve the accuracy of positioning various types of objects in space, air, and underwater spaces is of priority scientific and practical importance and involves an increasing number of researchers and practitioners who tackle it. The difference in the physical properties of the environment of various types of objects has led to the need to devise a wide range of mathematical methods, hardware and software tools for solving this task. Despite the successes achieved, a systematic solution to this problem has not yet been found. Increasing the frequency range in radar, radio navigation and modern mobile radio communication systems has significantly increased the accuracy of geolocation of radio sources, but this has led to a limitation of the radar range to the "line of sight" range. The "line of sight" limitation also applies to the infrared and optical frequency ranges. Systematic and random errors in the results of video observations of optical-electronic stations (OESs) along the trajectories of aircraft (AC) have led to the fact that instead of estimating the exact location of AC in the airspace for each moment of time, it is possible to estimate only the boundaries of the uncertainty region in which, with a given probability, the AC is located. The shape and boundaries of this region depend not only on the errors in the results of video observations but also on many additional factors: the relative spatial location of the

AC and each *i*-th OES; time of day and weather conditions; method of positioning the AC in the airspace. Currently, the main form of assessing the accuracy of positioning an AC in the airspace is the scattering ellipsoid, which corresponds to the hypothesis of the normality of the laws of distribution of estimates of the location of AC in the airspace. Under real conditions, this hypothesis is not always confirmed, which leads to the fact that the scattering ellipsoid is a special case of approximation of the actual area in which the aircraft is located with a given probability. Thus, the task to assess the accuracy of aircraft positioning in the airspace for each fixed time point of video surveillance is extremely relevant both theoretically and practically.

2. Literature review and problem statement

Paper [1] is one of the first systematic studies of modern location methods. It considers various principles and scenarios of aircraft location, but the error analysis is limited to variance estimates. Similarly, in [2], which investigates UWB aircraft localization in open space, the authors demonstrate high accuracy of their proposed method but do not consider how errors are distributed in space. This limits the possibility of using the results reported in [2] to build probabilistic models.

Work [3] discusses the integration of multisensor systems and artificial intelligence for aircraft detection. The paper focuses on increasing the accuracy and efficiency of detection, but the error analysis is limited to qualitative characteristics without a detailed study of their distribution. A similar approach is found in [4], which uses Bayesian inference to detect aircraft using multisensor data. Although the authors mention the impact of noise on accuracy, the density of the error distribution remains beyond the scope of the study.

Many techniques of aircraft location are active, i.e., based on irradiation of the aircraft with any radiation with subsequent analysis of the reflected signal. Such methods have a significant drawback associated with the possibility of easy detection of the fact of location and the source of the location signal. Therefore, such methods have limited application under combat conditions. Optical methods of covert video surveillance of aircraft movement trajectories, which are based on the analysis of visual observation data of the aircraft and are not associated with the emission of any signal by the location station, are also actively developing. For example, in work [5], a real-time method for optical (visual) localization and tracking of aircraft is proposed, which is based on the approximation of the aircraft location area by an ellipse. In an earlier work [6], the same authors proposed the use of dynamic visual sensors DVS (which record not the image but its pixel-by-pixel change) for spatial localization of AC. These sensors have very high temporal resolution, which makes them particularly useful for tracking fast-moving objects. Both studies demonstrate high accuracy under controlled conditions, but do not analyze the error distribution, which makes it difficult to assess the reliability of the method when external factors change. In [7], neural networks are used for optical localization of AC, similarly focusing on processing speed but not on error statistics.

Whereas works [5–7] considered single-sensor systems, paper [8] investigated the localization of aircraft using distributed sensors. The authors' approach is based on cooperative measurements, which increases accuracy, but they do not consider both the errors of individual network nodes and the resulting location error. On the other hand, work [9] proposed a method for distributed error correction of a multi-sensor location model using the extended Kalman filter (EKF). Although the work addresses the problem of errors, the emphasis is on their minimization, rather than the analysis of their statistical properties, which could improve the adaptability of the algorithm.

Among the works reviewed, study [10] is closest to our topic. The authors analyze errors in distance-based AC localization algorithms and conduct experiments to assess their impact on location accuracy. They note that the errors depend on the geometry of the sensor locations and environmental conditions, but their analysis is limited to the mean values and variance without constructing the full density distribution. Similarly, paper [11], which investigates the joint use of radar and visual data for detecting aircraft at low altitudes, emphasizes the importance of the impact of noise on the accuracy of location without delving into the probabilistic characteristics of errors.

Many recent works [3, 12–14] emphasize the application of modern machine learning and artificial intelligence methods to analyze optical or multisensor location data, as well as to identify and classify aircraft under different measurement conditions. All of these works note the importance of accounting for noise and measurement errors, but no systematic analysis of the distribution of location errors is performed. In [12], an overview of approaches based on machine learning is provided to solve the problem of not only detecting aircraft in an image in the optical or infrared range but also distinguishing them from the point of view of friend or foe. In [13], the emphasis is on building machine learning models that allow for effective detection of aircraft in urban environments. In [14], the authors present a multisensor aircraft detector that combines optical and infrared video cameras with acoustic sensors. Data processing from all sensors is performed in a coordinated manner using artificial intelligence methods. In addition, in [14], an annotated database of video images and acoustic signals for different types of aircraft (drones, airplanes, helicopters) and birds is presented, taking into account various background noises. All these works note the importance of accounting for noise and measurement errors, but no systematic analysis of the distribution of location errors is performed. Moreover, it should be taken into account that the results of algorithms based on machine learning models and methods cannot be analyzed theoretically in most cases. In [15], an analytical method for assessing the accuracy of aircraft positioning using an OES network was devised. The authors also note the importance of accounting for measurement errors of each network OES but are limited to estimates of the mean value and variance of AC coordinates.

In [16], an overview of the main methods for positioning radio emission sources (RES) is given: time of arrival (TOA), time difference of arrival (TDOA), received signal strength (RSS), and direction of arrival (DOA) of the emitted signal. A comparative analysis of the positioning system is presented based on system characteristics and operational parameters, such as accuracy, the possibility of positioning in the line of sight (LOS) and beyond its limits (NLOS), the number of base stations required for positioning. The mean value and variance are used as indicators of system efficiency. To assess the limits of positioning accuracy, the circular probability deviation (CPD) metric and the Cramer-Rao

lower bound metric (CRLB), which is the lower bound of the variance of the estimation of RES coordinates, are used. It is shown that CRLB can be visualized by an error ellipse on a plane and allows one to estimate the magnitude and direction of the error. The CPD can be visualized by an error circle on a plane and allows one to estimate only the magnitude of the error. Both of these estimates are used under the assumption that the errors in the RES coordinate estimates have a normal distribution.

In [17], a method for increasing the accuracy of determining the object's coordinates by combining two small-sized radars into a network is considered. Elliptical uncertainty regions of open measurements for each radar are considered, and the intersection of these ellipses is proposed to be used as an estimate of the accuracy of determining the aircraft's coordinates. In [18], a method of passive location by an airborne infrared detection system using four infrared direction-finding sensors located in the head, tail, and wings of the carrier aircraft is considered. The target position is determined by the measured distance, azimuth angle, and position of the carrier aircraft. The authors investigate only point estimates of the target coordinates and their sensitivity to errors in measuring the angles of view of the relative location of the carrier aircraft and the object. Estimates of the accuracy of the target location are not given. In [19, 20], a description and individual characteristics of the equipment of cosmodromes, test ranges, and astronomical observatories equipped with the most modern optoelectronic, quantum-optical, laser-television means and systems of high-precision trajectory measurements are given. As their main metrological characteristics, only numerical values of SCR of the errors of measurements of azimuth, elevation angle, and inclined range are used, and as an estimate of the accuracy of the location of the aircraft, the scattering ellipsoid is also used. In [20], the metric of the CPD and the metric of the CRLB are used to estimate the limits of the accuracy of positioning RES, which under certain conditions gives a lower limit for the dispersion of the estimation of RES coordinates. It is shown that the CRLB can be visualized by an ellipse of errors on a plane and allows one to estimate the magnitude and direction of the error. The CPD can be visualized as a circle of errors on a plane and allows one to estimate only the magnitude of the error. Both of these estimates are used under the assumption that the errors in the estimates of the source coordinates have a normal distribution.

Modern research in the field of aircraft positioning demonstrates significant progress in the development of technologies and methods aimed at increasing the accuracy of determining their location in the airspace. However, despite the large body of research into various aspects of aircraft localization, one of the insufficiently studied topics is the problem of evaluating the statistical properties of errors in estimates of aircraft location coordinates in the airspace. Knowledge of these properties is of decisive importance for the construction of accurate and reliable localization methods and algorithms for processing the results of location measurements.

In most works, authors emphasize the importance of positioning accuracy for various applications but do not delve into the statistical analysis of the distribution of errors, limiting themselves to general metrics such as root mean square error (RMSE).

This highlights a gap in literature: even in works where errors are studied, their statistical nature remains insufficiently disclosed.

Thus, our review of the literature [1–20] shows that most of the research is focused on the development of new localization methods and increasing their accuracy, while the laws of distribution of coordinate determination errors remain insufficiently studied. At the same time, this information is critically important for building probabilistic models that could predict the behavior of errors in different conditions and improve localization algorithms. For example, knowledge of the laws of distribution of errors would make it possible to more accurately assess the shapes and boundaries of the uncertainty region in which, with a given probability, the aircraft is located. Only a few works, such as [10, 15, 20], touch on this topic, but they do not offer an exhaustive analysis. Thus, there is a clear insufficiency in studies of assessing the accuracy of aircraft positioning depending on a priori information about the law and parameters of the distribution of errors of aircraft location coordinates estimates in airspace for each moment of its video surveillance by the ICN of OES.

3. The aim and objectives of the study

The purpose of our study is to devise a method for assessing the accuracy of AC positioning in the form of a convex polyhedron, in which, with a given probability, the aircraft is located at each moment of its video surveillance by OES infocommunication network (ICN). Identifying the regularity of changes in the shapes and boundaries of the convex polyhedron depending on the errors of OES video surveillance and their spatial location relative to the aircraft makes it possible to increase the efficiency of assessing the accuracy of AC positioning and the effectiveness of using all types of means of defeating air targets under combat conditions.

To achieve the goal, the following tasks were set:

– to build simulation models of geopositioning of optical-electronic stations of open and covert video surveillance;

– to develop an algorithm for estimating errors in the coordinates of the location of aircraft;

– to evaluate the statistical properties of errors in estimates of the coordinates of the location of aircraft;

– to devise methods for constructing shapes and boundaries of the uncertainty region of the location of aircraft;

– to analyze the statistical properties of errors in estimating the coordinates of the aircraft location.

4. The study materials and methods

The object of our study is the accuracy of AC positioning in the airspace, the detection of patterns of their change depending on the statistical properties of direct measurements of OES video surveillance and the relative location of AC relative to OES.

The hypothesis of the study assumes that the statistical properties of random errors of aircraft positioning in the airspace change from normal distribution laws to the Student's t-distribution or the Johnson distribution S_U.

Adopted assumptions. It is assumed that the errors of all components of the video surveillance processes are random variables with a normal distribution law and known parameters. Airspace monitoring in the optical and infrared frequency ranges is carried out within the direct line of sight. It is assumed that the maximum values of the inclined range between OES and the aircraft are a priori known, at which at

each moment of its video surveillance the following functional tasks are solved:

– detection;

– classification;

– determination of location coordinates;

– high-precision tracking.

Estimates of AC location coordinates in the airspace relative to the location of OES were calculated using the methods discussed in [21]. The statistical properties of the errors of the aircraft location coordinates, depending on the variances of the errors of all the component processes of video surveillance, were calculated using a simulation model of open and covert video surveillance of OES ICN along the trajectory of AC. The calculation of estimates of the distribution laws of errors of the aircraft location coordinates and their parameters was carried out using the method of moments with the subsequent selection of approximating Johnson distributions and verification of the corresponding statistical hypotheses.

Accepted simplifications. When using the simulation model of covert video surveillance of OES ICN along the trajectory of the aircraft, it was assumed that the location coordinates of all OESs are a priori known. Moreover, for each fixed time point of video surveillance, it was assumed that the coordinates of the aircraft location are also known with an accuracy of their mathematical expectations.

The research was conducted using the Monte Carlo method, probability theory, mathematical statistics, and linear algebra and included:

1) calculating estimates of the mathematical expectations of the azimuth and elevation angle of the line of sight from each OES to AC based on known estimates of the mathematical expectations of the coordinates of OES and AC locations at each time point of its video surveillance;

2) calculating the results of direct measurements of azimuth, elevation angle, and slant range by generating random measurement errors according to the video surveillance simulation model;

3) calculating estimates of the AC location coordinates based on the results of direct measurements of azimuth and elevation angle;

4) calculation of AC location errors and formation of a training sample of a given volume N was carried out for each coordinate in the form of the difference between the obtained estimate and its mathematical expectation by repeating points 2–4 N times;

5) evaluation of the statistical properties of the errors of AC location coordinates estimates in the form of estimates of four central moments and the covariance matrix K, for which its eigenvectors and numbers were determined and a scattering ellipsoid with a given confidence probability was constructed;

6) analysis of the dependence of the statistical properties of AC location errors on the statistical properties of the instrumental means of direct measurements of OES and the trajectory of AC movement relative to the geopositioning of OES ICN.

The main study concerned obtaining the dependence of the statistical properties of AC location errors on the statistical properties of the instrumental means of direct measurements of OES and the trajectory of AC movement relative to the geopositioning of OES ICN by a numerical method.

The equipment used in the study was a prototype of OES with its metrological characteristics and proprietary specialized software [15].

For random variables (RVs) of their parameters and estimates in the study, the following notations were used: (Ω, B, P) – Cartesian product of probability spaces (Ω_i, B_i, P_i), $i = 1, 2, ..., n$ $(\Omega = \Omega_1 \times \Omega_2 \times ... \times \Omega_n;\ B = B_1 \times B_2 \times ... \times B_n;\ P = P_1 \times P_2 \times ... \times P_n)$; Ω_i – space of elementary events; B_i – σ-algebras of events with Ω_i; P_i – probability measures on B_i; C – deterministic value; $C(\omega)$ – random value, $\omega \in \Omega$; $\overline{c} = M_{\omega}\{C(\omega)\}$ – mathematical expectation of a random value; $\sigma_c^2 = M_{\omega}\{C(\omega) - \overline{c}\}^2$ – variance of a random value; $C(\tilde{\omega})$ – realization of a random value for a fixed $\tilde{\omega} \in \Omega$; $\hat{C}(\omega)$ – estimate of a random value; $C(\tilde{\omega}) \cong N(\overline{c}, \sigma_c^2)$ – normal distribution law of a random value $C(\omega)$ with mathematical expectation $\bar{c}$ and variance σ_c^2.

As hardware for the study, custom-built OESs [22] with software developed for them were used. Simulation modeling and rendering of three-dimensional scenes were performed in the GNU Octave environment.

5. Results of research on the numerical method for assessing the accuracy of AC positioning

5. 1. Construction of simulation models

5. 1. 1. Simulation model of geopositioning of optoelectronic stations in the infocommunication network

Each i-th OES ICN is equipped with a GNSS signal receiver for its geopositioning, designed for automatic continuous estimation of current coordinates, road speed and time using GNSS GPS/GLONASS radio signals at any point on the globe, at any time, regardless of weather conditions. Simultaneously with the solution of the main navigation task, the receiver ensures the reception and consideration of differential corrections (when operating under a differential mode) and provides measurement of the coordinates of the location of each i-th OES ICN on the earth's surface with an accuracy of up to the first two central moments. The mean square deviation (MSD) of coordinate determination errors: autonomous – 1.5 m; under a differential mode less than 0.5 m. Thus, as a result of geopositioning of each i-th OES ICN, a pair of vectors is obtained $\left(\hat{\tilde{X}}_{i0}(\omega), \hat{\tilde{Y}}_{i0}(\omega), \hat{\tilde{Z}}_{i0}(\omega)\right)^T$, $\left(\hat{\tilde{L}}_{i0}(\omega), \hat{\tilde{B}}_{i0}(\omega), \hat{\tilde{H}}_{i0}(\omega)\right)^T$ – estimates of mathematical expectations of the coordinates of the location of the i-th OES ICN in the global coordinate system (GCS) and in WGS-84. In the future, the value of the MSD is taken as 1 m for each of the three coordinates. The GCS and WGS-84 coordinate systems are functionally related to each other. It is known [23] that the direct transition from geodetic coordinates $\left(\hat{\tilde{L}}_{i0}(\omega), \hat{\tilde{B}}_{i0}(\omega), \hat{\tilde{H}}_{i0}(\omega)\right)^T$ – given in the WGS-84 system to $\left(\hat{\tilde{X}}_{i0}(\omega), \hat{\tilde{Y}}_{i0}(\omega), \hat{\tilde{Z}}_{i0}(\omega)\right)^T$ in GCS is carried out by a standard analytical method, and the calculation of geodetic coordinates $\left(\hat{\tilde{L}}_{i0}(\omega), \hat{\tilde{B}}_{i0}(\omega), \hat{\tilde{H}}_{i0}(\omega)\right)^T$ is performed iteratively.

To model the errors of the geolocation results of each i-th OES in GCS, we shall use a simulation model, which is represented in the form:

$$X_{i0}(\tilde{\omega}) \cong N\left(\hat{\tilde{X}}_{i0}(\omega), \sigma_{X_i}^2\right), \quad (1)$$

$$Y_{i0}(\tilde{\omega}) \cong N\left(\hat{\tilde{Y}}_{i0}(\omega), \sigma_{Y_i}^2\right), \quad (2)$$

$$Z_{i0}(\tilde{\omega}) \cong N\left(\hat{\tilde{Z}}_{i0}(\omega), \sigma_{Z_i}^2\right), \quad (3)$$

where $\left(\hat{\bar{X}}_{i0}(\omega), \hat{\bar{Y}}_{i0}(\omega), \hat{\bar{Z}}_{i0}(\omega)\right)^T$, $\left(\sigma^2_{X_i}, \sigma^2_{Y_i}, \sigma^2_{Z_i}\right)^T$ are the vectors of mathematical expectations and variances of random errors of the geopositioning results of each *i*-th OES in GCS.

In [15], the sources of systematic errors in measuring the azimuth and elevation angle of AC and methods for their compensation were considered, therefore, in this work, the influence of systematic errors is not considered.

5. 1. 2. Simulation model of open video surveillance

When detecting, capturing, and tracking AC OES ICN during open video surveillance, each *i*-th OES measures three parameters: azimuth $\alpha_{ij}(\omega)$, elevation angle $\beta_{ij}(\omega)$, and slant range $D_{ij}(\omega)$ to the *j*-th AC. If the frame rate of video cameras is *k* frames per second (the frequency of measuring azimuth and elevation angle), and the parameters of AC trajectory are estimated with a frequency of once per second, then the vector of estimates of mathematical expectations of AC $\left(\hat{\bar{\alpha}}_{ij}(\omega), \hat{\bar{\beta}}_{ij}(\omega), \hat{\bar{D}}_{ij}(\omega)\right)^T$, obtained by averaging the results of measuring azimuth and elevation angle by *k* is used as the vector of measured parameters. In this case, the vector $\left(\hat{\bar{\alpha}}_{ij}(\omega), \hat{\bar{\beta}}_{ij}(\omega), \hat{\bar{D}}_{ij}(\omega)\right)^T$ determines the location of AC in the instrumental Cartesian coordinate system (ICCS) of the OES. Estimates of the variance of errors of direct measurements of azimuth $\sigma^2_{\alpha_i}(\omega)$, elevation angle $\sigma^2_{\beta_i}(\omega)$, and slant range $\sigma^2_{D_i}(\omega)$ of each *i*-th OES ICN are assumed to be known a priori. When constructing a simulation model of open video surveillance of AC, it is assumed that the random errors of direct measurements $\alpha_{ij}(\omega)$, $\beta_{ij}(\omega)$, and $D_{ij}(\omega)$ are distributed according to the normal law. In this case, the simulation model of the observation errors of the *j*-th AC of each *i*-th OES takes the form:

$$\alpha_{ij}(\tilde{\omega}) \cong N\left(\hat{\bar{\alpha}}_{ij}(\omega), \sigma^2_{\alpha_i}\right), \quad (4)$$

$$\beta_{ij}(\tilde{\omega}) \cong N\left(\hat{\bar{\beta}}_{ij}(\omega), \sigma^2_{\beta_i}\right), \quad (5)$$

$$D_{ij}(\tilde{\omega}) \cong N\left(\hat{\bar{D}}_{ij}(\omega), \sigma^2_{D_i}\right), \quad (6)$$

where $\left(\hat{\bar{\alpha}}_{ij}(\omega), \hat{\bar{\beta}}_{ij}(\omega), \hat{\bar{D}}_{ij}(\omega)\right)^T$, $\left(\sigma^2_{\alpha_i}(\omega), \sigma^2_{\beta_i}(\omega), \sigma^2_{D_i}(\omega)\right)^T$ are the vectors of mathematical expectations and variances of random errors of direct measurements of azimuth, elevation angle, and inclined range. The components of the vector of estimates of the coordinates of the location of the *j*-th AC $\left(\hat{\bar{x}}_j(\omega), \hat{\bar{y}}_j(\omega), \hat{\bar{z}}_j(\omega)\right)^T$ in the ICCS of OES are determined by the following expressions [15]:

$$\hat{\bar{x}}_j(\omega) = \hat{\bar{D}}_{ij}(\omega)\cos\hat{\bar{\beta}}_{ij}(\omega)\cos\hat{\bar{\alpha}}_{ij}(\omega), \quad (7)$$

$$\hat{\bar{y}}_j(\omega) = \hat{\bar{D}}_{ij}(\omega)\sin\hat{\bar{\beta}}_{ij}(\omega), \quad (8)$$

$$\hat{\bar{z}}_j(\omega) = \hat{\bar{D}}_{ij}(\omega)\cos\hat{\bar{\beta}}_{ij}(\omega)\sin\hat{\bar{\alpha}}_{ij}(\omega). \quad (9)$$

The vector $\left(\hat{\bar{x}}_j(\omega), \hat{\bar{y}}_j(\omega), \hat{\bar{z}}_j(\omega)\right)^T$ is considered as an estimate of the mathematical expectations of the coordinates of the location of the *j*-th AC in the ICCS of the *i*-th OES. For practical use of the results of video observations of AC trajectory, it is necessary to transform the coordinates of the location of AC from the ICCS of OES to the global Cartesian coordinate system GCS. The model for recalculating the vector of coordinates of the location of AC from ICCS – the *i*-th OES into a vector of estimated coordinates $(X_j(\omega), Y_j(\omega), Z_j(\omega))^T$ of the location of the *j*-th AC in GCS has the form [15]

$$\begin{Vmatrix} X_{jo}(\omega) \\ Y_{jo}(\omega) \\ Z_{jo}(\omega) \end{Vmatrix} = \mathbf{A}_i(\boldsymbol{\omega}) \cdot \begin{Vmatrix} \hat{\bar{x}}_j(\omega) \\ \hat{\bar{y}}_j(\omega) \\ \hat{\bar{z}}_j(\omega) \end{Vmatrix} + \begin{Vmatrix} \hat{\bar{X}}_{i0}(\omega) \\ \hat{\bar{Y}}_{i0}(\omega) \\ \hat{\bar{Z}}_{i0}(\omega) \end{Vmatrix}, \quad (10)$$

The transformation matrix $\mathbf{A}_i(\omega)$ takes the form

$$\mathbf{A}_i(\boldsymbol{\omega}) = \begin{Vmatrix} -\cos\hat{\bar{L}}_{i0}(\omega)\cdot\sin\hat{\bar{B}}_{i0}(\omega) & \cos\hat{\bar{L}}_{i0}(\omega)\cdot\cos\hat{\bar{B}}_{i0}(\omega) & -\sin\hat{\bar{L}}_{i0}(\omega) \\ -\sin\hat{\bar{L}}_{i0}(\omega)\cdot\sin\hat{\bar{B}}_{i0}(\omega) & \sin\hat{\bar{L}}_{i0}(\omega)\cdot\cos\hat{\bar{B}}_{i0}(\omega) & \cos\hat{\bar{L}}_{i0}(\omega) \\ \cos\hat{\bar{B}}_{i0}(\omega) & \sin\hat{\bar{B}}_{i0}(\omega) & 0 \end{Vmatrix}, \quad (11)$$

where, as before, $\left(\hat{\bar{L}}_{i0}(\omega), \hat{\bar{B}}_{i0}(\omega), \hat{\bar{H}}_{i0}(\omega)\right)^T$ is the vector of estimates of the mathematical expectations of the coordinates of the location of the *i*-th OES in WGS-84. During open video surveillance of the trajectory of AC movement *n* OES ICN, *n* estimates of the coordinates of AC location $\left(\hat{\bar{x}}_j(\omega), \hat{\bar{y}}_j(\omega), \hat{\bar{z}}_j(\omega)\right)^T$, $i = 1, 2, \ldots, n$ are obtained. Since the *j*-th AC is located at different distances from each *i*-th OES, the estimates $\left(\hat{\bar{x}}_j(\omega), \hat{\bar{y}}_j(\omega), \hat{\bar{z}}_j(\omega)\right)^T$, $i = 1, 2, \ldots, n$ must be considered as the results of indirect, unequally accurate measurements. In this case, the estimates of the mathematical expectation of the coordinates of the location of the *j*-th AC in GCS for open video surveillance are equal to:

$$\bar{X}_{jo}(\omega) = \sum_{i=1}^{n} W_{X_j} X_j(\omega) \Big/ \sum_{i=1}^{n} W_{X_j}, \quad (12)$$

$$\bar{Y}_{jo}(\omega) = \sum_{i=1}^{n} W_{Y_j} Y_j(\omega) \Big/ \sum_{i=1}^{n} W_{Y_j}, \quad (13)$$

$$\bar{Z}_{jo}(\omega) = \sum_{i=1}^{n} W_{Z_j} Z_j(\omega) \Big/ \sum_{i=1}^{n} W_{Z_j}, \quad (14)$$

where $W_{X_j} = 1 / \sigma^2_{X_j}$, $W_{Y_j} = 1 / \sigma^2_{Y_j}$, $W_{Z_j} = 1 / \sigma^2_{Z_j}$, $i = 1, 2, \ldots, n$.

Estimates of the variances of coordinates of the location of the *j*-th AC in GCS are equal to:

$$\sigma^2_{X_j} = 1 \Big/ \sum_{i=1}^{n} W_{X_j}, \quad \sigma^2_{Y_j} = 1 \Big/ \sum_{i=1}^{n} W_{Y_j}, \quad \sigma^2_{Z} = 1 \Big/ \sum_{i=1}^{n} W_{Z_j}. \quad (15)$$

Estimates of the weighted values of the coordinates of the location vector $\left(\bar{X}_j(\omega), \bar{Y}_j(\omega), \bar{Z}_j(\omega)\right)^T$ of the *j*-th AC in GCS, calculated according to (12) to (14), take into account the spatial redundancy of measurements of the coordinates of the location of AC ICN of OES, are less biased and more effective compared to the estimates obtained from each *i*-th OES.

5. 1. 3. Simulation model of covert video surveillance

When conducting trajectory measurements using the method of covert surveillance of location of the *j*-th AC for each time point *t* of the *i*-th OES, only two parameters are measured: azimuth $\hat{\bar{\alpha}}_{ij}(\omega)$, and elevation angle $\hat{\bar{\beta}}_{ij}(\omega)$.

When $\bar{D}_{ij}(\omega) = 1$, from (7) to (9) we obtain estimates of the mathematical expectations of the directional coefficients $\left(\hat{\bar{l}}_{ij}(\boldsymbol{\omega}), \hat{\bar{m}}_{ij}(\boldsymbol{\omega}), \hat{\bar{n}}_{ij}(\boldsymbol{\omega})\right)^T$ of the line of sight from the *i*-th OES to the *j*-th AC in ICCS:

$$\hat{\bar{l}}_{ij}(\boldsymbol{\omega}) = \cos\hat{\bar{\beta}}_{ij}(\omega)\cos\hat{\bar{\alpha}}_{ij}(\omega), \quad (16)$$

$$\hat{\boldsymbol{m}}_{ij}(\boldsymbol{\omega}) = \sin\hat{\beta}_{ij}(\omega), \quad (17)$$

$$\hat{\boldsymbol{n}}_{ij}(\boldsymbol{\omega}) = \cos\hat{\beta}_{ij}(\omega)\sin\hat{\alpha}_{ij}(\omega), \quad (18)$$

where, as before, $\left(\hat{\alpha}_{ij}(\omega), \hat{\beta}_{ij}(\omega)\right)^T$ are the estimates of the mathematical expectations of the azimuth and elevation angle from the i-th OES to the j-th AC in ICCS. The vector $\left(\hat{\bar{l}}_{ij}(\omega), \hat{\bar{m}}_{ij}(\omega), \hat{\bar{n}}_{ij}(\omega)\right)^{\mathrm{T}}$ of mathematical expectations of the directional coefficients of the line of sight from the i-th OES to the j-th AC in GCS is equal to

$$\begin{Vmatrix} \hat{\bar{l}}_{ij}(\omega) \\ \hat{\bar{m}}_{ij}(\omega) \\ \hat{\bar{n}}_{ij}(\omega) \end{Vmatrix} = \mathbf{A}_i(\boldsymbol{\omega}) \cdot \begin{Vmatrix} \hat{\bar{l}}_{ij}(\boldsymbol{\omega}) \\ \hat{\bar{m}}_{ij}(\boldsymbol{\omega}) \\ \hat{\bar{n}}_{ij}(\boldsymbol{\omega}) \end{Vmatrix}, \quad (19)$$

where, as before, $\left(\hat{\bar{l}}_{ij}(\boldsymbol{\omega}), \hat{\bar{m}}_{ij}(\boldsymbol{\omega}), \hat{\bar{n}}_{ij}(\boldsymbol{\omega})\right)^{\mathrm{T}}$ is the vector of estimates of the mathematical expectations of the direction coefficients of the line of sight from the i-th OES to the j-th AC in ICCS; $\mathbf{A_i}(\omega)$ is the matrix of the transformation of ICCS of the i-th OES into GCS of the form (11). To simplify the writing of the simulation model, the following notations are introduced. The ICN consists of N spatially separated OESs, which are located at points with coordinates $\vec{P}_{i0} = \left(\hat{\bar{X}}_{i0}(\omega), \hat{\bar{Y}}_{i0}(\omega), \hat{\bar{Z}}_{i0}(\omega)\right)^{\mathrm{T}}$, and the lines of sight from the i-th OES to the j-th AC, which is located at point $\vec{T}_j = \left(\bar{X}_j(\omega), \bar{Y}_j(\omega), \bar{Z}_j(\omega)\right)^{\mathrm{T}}$, are given by their direction coefficients of the lines of sight

$$\vec{L}_{ij} = \left(\hat{\bar{l}}_{ij}(\omega), \hat{\bar{m}}_{ij}(\omega), \hat{\bar{n}}_{ij}(\omega)\right)^T, \quad \left|\vec{L}_{ij}\right| = 1, \quad (20)$$

where $i = 1, 2, \ldots, N; j = 1, 2, \ldots, M$.

Then the equations of the lines of sight from the i-th OES to the j-th AC can be represented as

$$\left(\vec{P}_{i0}, \vec{L}_{ij}\right) = \vec{P}_{i0} + t\vec{L}_{ij}, \quad (21)$$

where $i = 1, 2, \ldots, N; j = 1, 2, \ldots, M$.

To determine the spatial coordinates of the location of the j-th AC during video surveillance of it by n OES, it is necessary to find the intersection point of all n lines of sight. Under real conditions, due to measurement errors, the lines of sight for any n almost certainly do not intersect in space, therefore, as the desired position of the j-th AC in the airspace, we shall take the point $\vec{P}_{jco} = \left(X_{jco}(\omega), Y_{jco}(\omega), Z_{jco}(\omega)\right)^{\mathrm{T}}$, for which the sum of the squares of the distances to all lines of sight $\left(\vec{P}_{i0}, \vec{L}_{ij}\right)$ will be minimal

$$\vec{P}_{jco} = \arg\min_{(X_j, Y_j, Z_j)} \sum_{i=1}^{N} d\left(\vec{P}_{jco}, \left(\vec{P}_{i0}, \vec{L}_{ij}\right)\right)^2, \quad (22)$$

where the distance between an arbitrary point $\vec{P}_{jco}$ and the line given in the form (21) can be written as

$$d\left(\vec{P}_{jc0}, \left(\vec{P}_{i0}, \vec{L}_{ij}\right)\right) = \frac{\left|\vec{L}_{ij} \times \left(\vec{P}_{jco} - \vec{P}_{i0}\right)\right|}{\left|\vec{L}_{ij}\right|} = \left|\vec{L}_{ij} \times \left(\vec{P}_{jco} - \vec{P}_{i0}\right)\right|. \quad (23)$$

Formally, problem (22) is reduced to solving a system of linear algebraic equations

$$\mathbf{A}\vec{P}_{jco} = \vec{\mathrm{b}}. \quad (24)$$

Or, equivalently, to the inverse of the matrix

$$\vec{P}_{jco} = \mathbf{A}^{-1}\vec{\mathrm{b}}, \quad (25)$$

where

$$\mathbf{A} = \sum_{i=1}^{N} \mathbf{A}_i, \quad \vec{\mathrm{b}} = \sum_{i=1}^{N} \vec{\mathrm{b}}_i, \quad \mathbf{A}_i = \left(\mathbf{I} - \vec{L}_{ij}\vec{L}_{ij}^T\right), \quad \vec{\mathrm{b}}_i = \mathbf{A}_i\vec{P}_{i0}.$$

The resulting solution $\vec{P}_{jco} = \left(X_{jco}(\omega), Y_{jco}(\omega), Z_{jco}(\omega)\right)^{\mathrm{T}}$, is taken as an estimate of the coordinates of the location of the j-th AC in GCS for covert video surveillance.

5. 2. Algorithm for estimating errors in AC location coordinates

To estimate the statistical properties of errors in AC location coordinates, it is necessary to form representative error samples for open and covert video surveillance based on the constructed simulation models. Simulation models of video surveillance of OES ICN along the trajectory of AC were implemented using the statistical testing method using the following algorithm.

As initial data, a priori known estimates of mathematical expectations of the coordinates of the geopositioning of OES ICN (points $\vec{P}_i$, $i = 1, 2, \ldots, N$) on the earth's surface and the coordinates of the location of each j-th AC in the airspace (points $\vec{T}_j$, $j = 1, 2, \ldots, M$), as well as estimates of the dispersions of direct measurements of the coordinates of the geopositioning of OES, azimuth, elevation angle, and inclined range were used.

Algorithm:

1. The calculation of the direction vectors $\vec{L}_{ij}$ ($i = 1, 2, \ldots, N$) of the sighting lines of each i-th OES located at point $\vec{P}_{i0} = \left(\hat{\bar{X}}_{i0}(\omega), \hat{\bar{Y}}_{i0}(\omega), \hat{\bar{Z}}_{i0}(\omega)\right)^{\mathrm{T}}$, on the j-th AC located at point $\vec{T}_j = \left(\bar{X}_j(\omega), \bar{Y}_j(\omega), \bar{Z}_j(\omega)\right)^{\mathrm{T}}$ in GCS is carried out according to the expression

$$\vec{L}_{ij} = \frac{\vec{T}_j - \vec{\mathrm{P}}_{i0}}{\left|\vec{T}_j - \vec{\mathrm{P}}_{i0}\right|} = \left(\hat{\bar{l}}_{ij}(\omega), \hat{\bar{m}}_{ij}(\omega), \hat{\bar{n}}_{ij}(\omega)\right)^T. \quad (26)$$

2. Calculation of direction vectors

$$\vec{\boldsymbol{L}}_{ij} = \left(\hat{\bar{l}}_{ij}(\boldsymbol{\omega}), \hat{\bar{\boldsymbol{m}}}_{ij}(\boldsymbol{\omega}), \hat{\bar{\boldsymbol{n}}}_{ij}(\boldsymbol{\omega})\right)^{\mathrm{T}}$$

of the sighting lines of each i-th OES on the j-th AC in ICCS

$$\vec{\boldsymbol{L}}_{ij} = \begin{Vmatrix} \hat{\bar{l}}_{ij}(\boldsymbol{\omega}) \\ \hat{\bar{\boldsymbol{m}}}_{ij}(\boldsymbol{\omega}) \\ \hat{\bar{\boldsymbol{n}}}_{ij}(\boldsymbol{\omega}) \end{Vmatrix} = \mathbf{A}_i^T(\omega) \cdot \begin{Vmatrix} \hat{\bar{l}}_{ij}(\omega) \\ \hat{\bar{m}}_{ij}(\omega) \\ \hat{\bar{n}}_{ij}(\omega) \end{Vmatrix}. \quad (27)$$

3. Calculation of estimates of mathematical expectations of azimuth, elevation angle, and slant range from each i-th OES on j-th AC in ICCS. Estimates of the directional coefficients $\vec{\boldsymbol{L}}_{ij}$ of the line of sight from the i-th OES on j-th AC are related to estimates of azimuth, elevation angle, and slant range by expressions (26) to (28). From (27), (28) the following estimates are obtained

$$\hat{\bar{\beta}}_{ij}(\omega) = \arcsin\left(\hat{\bar{m}}_{ij}(\omega)\right), \quad (28)$$

where:

$$-\frac{\pi}{2}\le\beta_{ij}\le+\frac{\pi}{2},\ \left|\hat{\tilde{m}}_{ij}(\omega)\right|<1,$$

$$\hat{\tilde{\alpha}}_{ij}(\omega)=\arctan\left(\frac{\hat{\tilde{n}}_{ij}(\omega)}{\hat{\tilde{l}}_{ij}(\omega)}\right). \quad (29)$$

Since during the calculation of (29) the angle value will be in the range $(-\pi/2, +\pi/2)$, then to obtain the azimuth in the range $[0, 2\pi)$ it is necessary to specify

$$\hat{\tilde{\alpha}}_{ij}(\omega)=\begin{cases}\arctan\left(\hat{\tilde{n}}_{ij}(\omega)/\hat{\tilde{l}}_{ij}(\omega)\right), & \hat{\tilde{l}}_{ij}(\omega)>0\wedge\hat{\tilde{n}}_{ij}(\omega)\ge 0,\\ \arctan\left(\hat{\tilde{n}}_{ij}(\omega)/\hat{\tilde{l}}_{ij}(\omega)\right)+2\pi, & \hat{\tilde{l}}_{ij}(\omega)>0\wedge\hat{\tilde{n}}_{ij}(\omega)<0,\\ \arctan\left(\hat{\tilde{n}}_{ij}(\omega)/\hat{\tilde{l}}_{ij}(\omega)\right)+\pi, & \hat{\tilde{l}}_{ij}(\omega)<0,\\ +\frac{\pi}{2}, & \hat{\tilde{l}}_{ij}(\omega)=0\wedge\hat{\tilde{n}}_{ij}(\omega)>0,\\ +3\frac{\pi}{2}, & \hat{\tilde{l}}_{ij}(\omega)=0\wedge\hat{\tilde{n}}_{ij}(\omega)<0.\end{cases}$$

The calculation of the estimates of mathematical expectations of the inclined range from each *i*-th OES on AC is calculated as

$$\hat{\tilde{D}}_{ij}(\omega)=\sqrt{\left(\hat{\tilde{X}}_j(\omega)-\hat{\tilde{X}}_{i0}(\omega)\right)^2+\left(\hat{\tilde{Y}}_j(\omega)-\hat{\tilde{Y}}_{i0}(\omega)\right)^2+\left(\hat{\tilde{Z}}_j(\omega)-\hat{\tilde{Z}}_{i0}(\omega)\right)^2}. \quad (30)$$

4. The calculation of the geopositioning coordinates of each *i*-th OES ICN $i = 1, 2, ..., N$ was carried out using the simulation model (1) to (3) by generating *N* triples of random numbers with the parameters specified in the model. The obtained values $\left(X_{i0}(\tilde{\omega}), Y_{i0}(\tilde{\omega}), Z_{i0}(\tilde{\omega})\right)^T$ were taken as the results of direct measurements of the geopositioning coordinates of each *i*-th OES ICN in GCS with their subsequent conversion into geodetic coordinates $\left(L_{i0}(\tilde{\omega}), B_{i0}(\tilde{\omega}), H_{i0}(\tilde{\omega})\right)^T$, $i = 1, 2, ..., n$.

5. The calculation of the results of direct measurements $\alpha_{ij}(\tilde{\omega})$, $\beta_{ij}(\tilde{\omega})$, $D_{ij}(\tilde{\omega})$ from each *i*-th OES to the *j*-th AC was carried out by generating *n* triplets of random values using the simulation model (4) to (6).

6. Calculation of vectors $\left(x_{ij}(\tilde{\omega}), y_{ij}(\tilde{\omega}), z_{ij}(\tilde{\omega})\right)^T$ of the location coordinates of the *j*-th AC in ICCS of each *i*-th OES during *open* video surveillance according to (7) to (9).

7. Calculation of vectors $\left(X_j(\tilde{\omega}), Y_j(\tilde{\omega}), Z_j(\tilde{\omega})\right)^T$ of coordinates of the location of the *j*-th AC in GCS based on the results of video surveillance of each *i*-th OES $i = 1, 2, ..., n$ according to (10).

8. Calculation of vectors $\left(\bar{X}_j(\omega), \bar{Y}_j(\omega), \bar{Z}_j(\omega)\right)^T$ of weighted coordinates of the location of AC in GCS based on the results of *open* video surveillance of it by *n* OES according to (12) to (14) and their dispersions according to (15).

9. Calculation of vector $\left(X_{jco}(\omega), Y_{jco}(\omega), Z_{jco}(\omega)\right)^T$ of coordinates of the location of AC in GCS based on the results of *covert* video surveillance of it by *n* OES is performed in a number of stages:

1) calculation of *n* directional coefficients $\hat{\tilde{\boldsymbol{l}}}_{ij}(\boldsymbol{\omega})$, $\hat{\tilde{\boldsymbol{m}}}_{ij}(\boldsymbol{\omega})$, $\hat{\tilde{\boldsymbol{n}}}_{ij}(\boldsymbol{\omega})$ of the line of sight from each *i*-th OES to the *j*th AC in ICCS was carried out based on the results of *direct* measurements of $\hat{\tilde{\alpha}}_{ij}(\omega)$, $\hat{\tilde{\beta}}_{ij}(\omega)$, obtained in p. 5;

2) calculation of *n* directional coefficients $\left(\hat{\tilde{l}}_{ij}(\omega), \hat{\tilde{m}}_{ij}(\omega), \hat{\tilde{n}}_{ij}(\omega)\right)^T$ of the line of sight from each *i*-th OES $i = 1, 2, ..., n$ on the *j*-th AC in GCS according to (19);

3) formation (24) and solution (25) of the redefined system of linear algebraic equations of the line of sight of problem (22) and obtaining a vector of estimates of coordinates $\left(X_{jco}(\omega), Y_{jco}(\omega), Z_{jco}(\omega)\right)^T$ of the AC location in GCS based on the results of covert video surveillance of it by *n* OES.

10. Visualization of the results of estimates of the coordinates of the location of the *j*-th AC in GCS by the methods of open and covert video surveillance was carried out in three-dimensional space for visual analysis of the shape and size of the uncertainty regions of the results of estimates of the coordinates of the location of the *j*-th AC by the considered methods.

11. Calculation of error vectors of the location coordinates of the *j*-th AC is carried out separately for open $\mathbf{X}_{ok}$ and covert $\mathbf{X}_{cok}$ video surveillance by calculating the difference between the corresponding vectors $\left(\bar{X}_{jo}(\omega), \bar{Y}_{jo}(\omega), \bar{Z}_{jo}(\omega)\right)^T$, $\left(X_{jco}(\omega), Y_{jco}(\omega), Z_{jco}(\omega)\right)^T$ of the location coordinates of the *j*-th AC, estimated by simulation models, and the true location coordinates $\left(\hat{\tilde{X}}_j(\omega), \hat{\tilde{Y}}_j(\omega), \hat{\tilde{Z}}_j(\omega)\right)^T$ of the *j*-th AC.

12. The formation of training samples X_o and X_{co} (matrices of dimensionality $K \times 3$) of errors in the coordinates of the location of the *j*-th AC, estimated by the method of open X_o and hidden X_{co} video surveillance, is carried out by repeating $K > 1000$ times items 4–11 with saving the results.

5. 3. Estimation of statistical properties of errors in estimates of AC location coordinates

The training samples X_o and X_{co} are matrices of dimensionality $K \times 3$ of realizations of three-dimensional random variables of errors in the location coordinates of the *j*-th AC in GCS. Estimation of statistical properties of a three-dimensional random variable is reduced to the estimation of a series of one-dimensional random variables. The simplest option is to estimate the statistical properties of errors in the coordinates of the *j*-th AC independently for each of the coordinates (each column of the matrices X_o and X_{co}). To eliminate the correlation between coordinate errors, the following transformations were performed:

1. Based on the matrix X_o, a sample covariance matrix K_o is constructed.

2. The eigenvectors v_i and eigenvalues λ_i ($i = 1, 2, 3$) of the matrix K_o are found and arranged in descending order so that the largest eigenvalue λ_1 and the corresponding vector $\mathbf{v}_1$ correspond to index 1, and the minimum ones correspond to λ_3 and $\mathbf{v}_3$.

3. The vector $\mathbf{v} = (v_1, v_2, v_3)$ is considered as the error vector of the location of the AC coordinates, with the component v_1 determining the direction of the maximum error.

4. All row vectors X_{ok} $k = 1, 2, ..., K$ are projected onto directions $\mathbf{v}_i$ ($i = 1, 2, 3$)

$$X_{ik}=\left(X_{ik}, \mathbf{v}_i\right)/\left|\mathbf{v}_i\right|,$$

and matrix X_o^p, is obtained in which all elements of each row (error coordinates) are uncorrelated with each other.

5. The calculations in points 1–4 are repeated for the matrix X_{co} and a matrix X_{co}^p with uncorrelated elements of each row is obtained. Analysis of the statistical properties of

the positioning coordinate errors of the *j*-th AC is performed for each coordinate (column) of matrices X_o^p and X_{co}^p, considering them as training samples for one-dimensional random variables.

To evaluate the statistical properties of one-dimensional random variables, the method of moments is used. It is known [24] that the theoretical moments of the laws of distribution of random variables are expressed in terms of the parameters of their distribution. For one-dimensional distribution laws, expressions of some moments in terms of the parameters of the distribution are given in [24]. The idea of the method of moments is to equate theoretical and empirical moments. As many equations are composed as there are unknown parameters to be estimated. The solution to the system of equations obtained is taken as an estimate of the unknown parameters. A necessary condition for using the method of moments is the identification of a specific law of distribution of the studied random variables or some curve that approximates this law. Thus, the problem of identifying the law of probability distribution of random variables for the training sample arises. The simplest way to solve it is a simple search of possible known probability distributions with subsequent verification of the degree of adequacy of statistical criteria such as χ^2, Kolmogorov, Shapiro-Wilk, etc. If this fails, then one can approximate the empirical distribution law of the corresponding Johnson curve [24], who proposed three families of curves to approximate all known distribution laws (Fig. 1).

To estimate the parameters of the curve of each of the Johnson families, we can use the method of quantiles, the method of moments, the method of maximum likelihood, depending on what we know about RVs. If there is a large sample, then the use of all of the above methods will be quite effective. The probability density distribution of the family of Johnson distribution curves S_B with four parameters takes the form

$$f_{S_B}(x)=\frac{\eta}{\sqrt{2\pi}}\frac{\lambda}{(x-\varepsilon)\cdot(\lambda-x+\varepsilon)}\times \times\exp\left(-\frac{1}{2}\left[\gamma+\eta\cdot\ln\left(\frac{x-\varepsilon}{\lambda-x+\varepsilon}\right)\right]^2\right), \quad (31)$$

where $\varepsilon\le x\le\varepsilon+\lambda$, $\eta>0$, $-\infty<\gamma<\infty$, $\lambda>0-\infty<\varepsilon<\infty$.

The probability density distribution of the family of Johnson (log-normal) distribution curves S_L with three parameters takes the form

$$f_{S_L}(x)=\frac{\eta}{\sqrt{2\pi}(x-\varepsilon)}\exp\left\{-\frac{1}{2}\eta^2\left[\frac{\gamma^*}{\eta}+\ln(x-\varepsilon)\right]^2\right\}, \quad (32)$$

where $x\ge\varepsilon$, $\eta>0$, $-\infty<\gamma^*<\infty$, $-\infty<\varepsilon<\infty$.

The probability density of the family of Johnson distribution curves S_U with four parameters takes the form

$$f_{S_U}(x)=\frac{\eta}{\sqrt{2\pi}}\frac{1}{\sqrt{(x-\varepsilon)^2+\lambda^2}}\times \times\exp\left[-\frac{1}{2}\left(\gamma+\eta\ln\left(\left(\frac{x-\varepsilon}{\lambda}\right)+\left[\left(\frac{x-\varepsilon}{\lambda}\right)^2+1\right]^{\frac{1}{2}}\right)\right)^2\right], \quad (33)$$

where $-\infty<x<\infty$, $\eta>0$, $-\infty<\gamma<\infty$, $\lambda>0-\infty<\varepsilon<\infty$.

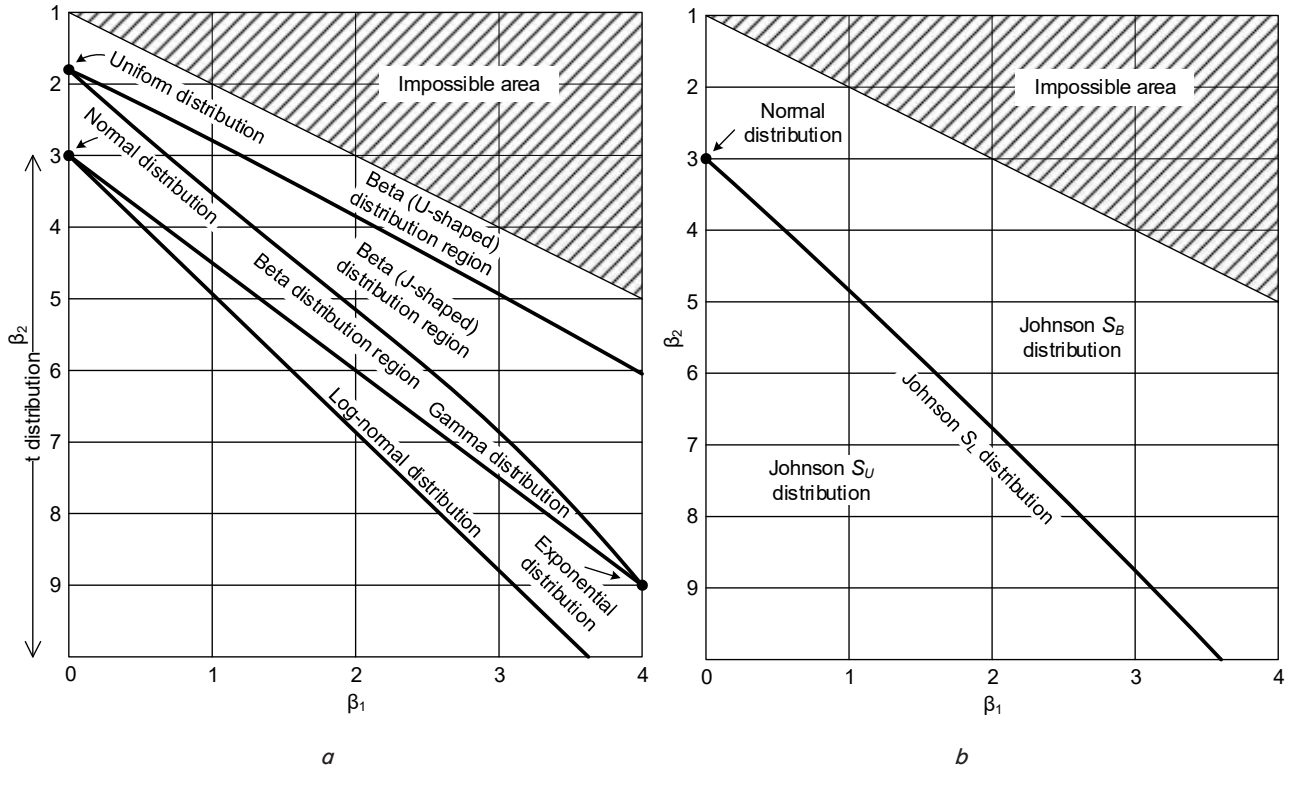

a *b*

Fig. 1. Approximation of the empirical law of distribution of one-dimensional random variables:
a — regions in the plane of normalized indices of asymmetry β_1 and kurtosis β_2;
b — three families of Johnson curves for approximation of all known one-dimensional laws of distribution of random variables

To apply the method of moments to estimate the parameters of the Johnson distribution for RV sample $\{x_i\}_{i=1,\dots,N}$, the following formulas are used to estimate the mathematical expectation, MSD, skewness and kurtosis coefficients:

$$m = \frac{1}{N}\sum_{i=1}^{N} x_i, \tag{34}$$

$$\sigma^2 = \frac{1}{N-1}\sum_{i=1}^{N}(x_i - m)^2, \tag{35}$$

$$\mu_3 = \frac{1}{N-1}\sum_{i=1}^{N}(x_i - m)^3, \tag{36}$$

$$\mu_4 = \frac{1}{N-1}\sum_{i=1}^{N}(x_i - m)^4, \tag{37}$$

$$\beta_1 = \frac{\mu_3^2}{\sigma^6},\ \beta_2 = \frac{\mu_4}{\sigma^4}, \tag{38}$$

where m is the mathematical expectation; σ is the standard deviation; μ_3, μ_4 are the third and fourth central moments.

5. 4. Method for constructing shapes and boundaries of the uncertainty region of AC location

The accuracy of AC location can be determined in the form of a certain spatial region in the airspace, in which, with a given probability, the AC is located for each fixed moment of its video surveillance. The assessment of the shape and boundary of such a region depends on a priori information about the statistical properties of the errors in the estimates of AC location coordinates at the same time. In radar, radio navigation, in mobile communication networks, in optical and optoelectronic systems, the main form of assessing the accuracy of location of a radio source or any other observed object is the scattering ellipsoid (SE). The theoretical basis for using the SE is the hypothesis of the normality of the law of distribution of errors in the estimates of the coordinates of the location of the object under study. Accepting this hypothesis, it is possible to estimate the magnitude and direction of the errors along the main axes of SE.

For effective use of SE in assessing the accuracy of AC location, it is necessary to either accept the hypothesis of the normality of the error distribution law or determine the conditions under which this hypothesis would not contradict the results of AC location assessment. Under actual conditions, this is quite difficult to do, therefore, a method is proposed for estimating the shape and boundaries of such a region with minimal available a priori information about the statistical properties of direct video surveillance errors based on the Chebyshev inequality.

To estimate the shape and boundaries of the uncertainty region of AC location, it is assumed that the density functions of the distribution of RVs of the video surveillance results are unknown, and only their first two moments are known: $\bar{\eta}$, σ_η^2 – the mathematical expectation and the variance. Then, for any positive $\varepsilon > 0$, the probability that the deviation of RV $\eta(\omega)$ from its mathematical expectation $\bar{\eta}$ in absolute value will be less than ε bounded from *below* by the value

$$P\left\{\left|\eta(\omega) - \bar{\eta}\right| \le \varepsilon\right\} \ge 1 - \frac{\sigma_\eta^2}{\varepsilon^2}. \tag{39}$$

Using (39), it is possible to estimate the lower and upper bounds of the uncertainty sector of the results of video observations of OES in azimuth, elevation angle, and slope range, within which, with a given probability, the true values of the results of video observations of the i-th OES for AC will be found. The lower and upper bounds of the errors of video observations are determined as follows:

– in azimuth $\alpha_i^- = \hat{\bar{\alpha}}_{it_k}(\omega) - k\hat{\sigma}_{\alpha_i}$, $\alpha_i^+ = \hat{\bar{\alpha}}_{it_k}(\omega) + k\hat{\sigma}_{\alpha_i}$;

– in elevation angle $\beta_i^- = \hat{\bar{\beta}}_{it_k}(\omega) - k\hat{\sigma}_{\beta_i}$, $\beta_i^+ = \hat{\bar{\beta}}_{it_k}(\omega) + k\hat{\sigma}_{\beta_i}$;

– in slope range $D_i^- = \hat{\bar{D}}_{it_k}(\omega) - k\hat{\sigma}_{\beta_i}$, $D_i^+ = \hat{\bar{D}}_{it_k}(\omega) + k\hat{\sigma}_{\beta_i}$.

Setting different values of k>1 and using Chebyshev's inequality (39), it is possible to obtain the upper and lower bounds of the uncertainty sector in azimuth, elevation angle, and slope range, in which the AC is located. For $k = 3$, the lower bound of the probability that the AC is inside the uncertainty sector takes the value $P \ge 0.8888\ldots$. If it is additionally known that the density function of the distribution of RV is symmetric from its mathematical expectation, the lower bound of the probability increases to $P \ge 0.9506$. For a normal distribution, the lower probability limit is $P \ge 0.9973$. The uncertainty sector boundaries are represented as corresponding linear inequalities that limit the azimuth error sector P_{i1} from below and P_{i2} from above

$$P_{i1} \ge 0: A_{i1}x + C_{i1}z \ge 0, \tag{40}$$

where $A_{i1} = -\sin\alpha_i^-$, $C_{i1} = \cos\alpha_i^-$;

$$P_{i2} \ge 0: A_{i2}x + C_{i2}z \ge 0, \tag{41}$$

where $A_{i2} = \sin\alpha_i^+$, $C_{i2} = -\cos\alpha_i^+$.

At the angle of place P_{i3} below and P_{i4} above:

$$P_{i3} \ge 0: A_{i3}x + B_{i3}y + C_{i3}z \ge 0, \tag{42}$$

$$P_{i4} \ge 0: A_{i4}x + B_{i4}y + C_{i4}z \ge 0, \tag{43}$$

where

$$A_{i3} = m_{i2}n_{i1} - m_{i1}n_{i2},\ B_{i3} = -\left(l_{i2}n_{i1} - l_{i1}n_{i2}\right),$$

$$C_{i3} = l_{i2}m_{i1} - l_{i1}m_{i2},\ A_{i4} = m_{i3}n_{i4} - m_{i4}n_{i3},$$

$$B_{i4} = -\left(l_{i3}n_{i4} - l_{i4}n_{i3}\right),\ C_{i4} = l_{i3}m_{i4} - l_{i4}m_{i3}.$$

Linear inequalities P_{i5} and P_{i6}, which limit the sector of errors in the inclined range from below and above, take the form:

$$P_{i5} \ge 0: A_{i5}x + B_{i5}y + C_{i5}z - D_{i5} \ge 0, \tag{44}$$

$$P_{i6} \ge 0: A_{i6}x + B_{i6}y + C_{i6}z - D_{i6} \ge 0, \tag{45}$$

where

$$A_{i5} = A_{i6} = \cos\beta_i\cos\alpha_i,\ B_{i5} = B_{i6} = \sin\beta_i,$$

$$C_{i5} = C_{i6} = \cos\beta_i\sin\alpha_i,\ D_{i5} = D_i^-,\ D_{i6} = D_i^+.$$

The error sector of open video surveillance S_i of the i-th OES is the inner region of the intersection of six half-spaces and is a convex polyhedral set

$$int(S_i) = \bigcap_{k=1}^{6} P_{ik}. \tag{46}$$

If at time t video surveillance of AC flight is carried out simultaneously by n OES ICN, then the shape and bound-

aries of the error region of the video surveillance results S_{Σ}^{o}, S_{Σ}^{h} are determined by the following expressions:

– for open surveillance

$$int\left(S_{\Sigma}^{o}\right)=\bigcap_{i=1}^{n}\bigcap_{k=1}^{6}P_{ik}; \quad (47)$$

– for covert surveillance

$$int\left(S_{\Sigma}^{h}\right)=\bigcap_{i=1}^{n}\bigcap_{k=1}^{6}P_{ik}. \quad (48)$$

In the following, regions (47) and (46) are termed Chebyshev forms and the boundaries of the uncertainty regions of AC location.

5. 5. Analysis of the statistical properties of errors in the estimates of AC location coordinates

5. 5. 1. Open video surveillance of one optoelectronic station

Analysis of the statistical properties of errors in the estimates of AC location coordinates was performed by the method of simulation modeling. The software implementation of the simulation models was performed in the GNU Octave environment using the Matgeom package and the GEOMLib library [25], which provides support for mesh based CSG (Composite Solid Geometry) operations. The convex polyhedron of the uncertainty region of AC position in space according to the data from OES was modeled in the form of a polygonal mesh. This allowed the use of CSG-intersection operations to form the final uncertainty region of AC location during observation by several OESs.

Visualization was performed in the global rectangular geocentric coordinate system XYZ, units of measurement are meters. To improve clarity and reduce the absolute values of the coordinates on plots, the origin of the coordinate system is conditionally shifted to the area of the location of OES, and the values are displayed relative to this local reference point.

To analyze the statistical properties of errors in determining the location of AC, simulation modeling was carried out for the AC at different distances and for different values of the deviation of errors in direct measurements of azimuth and elevation. High-precision video surveillance meets the standard metrological characteristics of OES and the minimum deviation of errors in direct video surveillance. Analysis of the statistical properties of AC location errors should answer the following question. Do nonlinear transformations of random variables (results of normally distributed video surveillance) lead to a significant deviation from the normal law of error distribution of estimates of each of the components of AC location coordinate vector? Studies allow us to establish threshold values of the MSD and distance to AC at which deviations from the normal law of distribution of errors in the estimates of each of the components of AC location coordinate vector become significant and must be taken into account.

Geopositioning of OESs – the coordinates of their location on the earth's surface $\left(\hat{\hat{X}}_{i0}(\omega), \hat{\hat{Y}}_{i0}(\omega), \hat{\hat{Z}}_{i0}(\omega)\right)^{T}$, $i=1, 2, ..., N$ and the coordinates of AC in the airspace $X=(X_j, Y_j, Z_j)^{T}$ were chosen by the researcher. Fig. 2 shows the actual and Chebyshev forms and boundaries of the uncertainty regions of AC location for different values of the inclined range $D=500$ m, 1000 m, 1500 m from the OES to the AC.

Simulation modeling of errors in video observation results for AC was performed using simulation models with a normal distribution law and the following parameters: MSD of geopositioning errors for each i-th OES in GCS $\sigma_{X_i}=\sigma_{Y_i}=\sigma_{Z_i}=0.5$ m; MSD of errors in direct measurements of azimuth, elevation angle, and slope range were taken equal to $\sigma_{\alpha}=0.1°$, $\sigma_{\beta}=0.1°$, $\sigma_{D}=1$ m. AC were located at distances of 1000, 5000, 10000, 15000, 20000, 25000, and 30000 meters.

Fig. 3 shows the actual Chebyshev forms and boundaries of uncertainty regions for AC location and the corresponding scattering ellipsoids for some values of slope range from OES to AC.

For open observation of one OES, the Chebyshev regions of uncertainty of AC location are convex polyhedral sets in the form of truncated tetrahedral pyramids with a constant height $h=6\sigma_D$. Fig. 4 shows values of the estimates β_1, β_2 for each component of AC location error vector. Fig. 5, 6 depict the distributions of AC location errors along each of the coordinate **v** of AC location error vector for distances of 15 km and 30 km at $\sigma_{\alpha}=\sigma_{\beta}=0.4°$. In the figures, their fit to the normal distribution law is indicated in red.

Analysis of the results shown in Fig. 4–6 allows us to conclude that with a deviation of direct measurements of azimuth and elevation angle not exceeding 0.1° and an inclined range of $\sigma_D=1$ m, the law of distribution of errors of AC location is well approximated by the normal one for each of the components of the vector of coordinates of AC location in the airspace. An increase in MSD leads to a significant deviation of the law of distribution of errors of the main component of AC location coordinates from the normal one towards the Johnson distribution S_U, while the remaining two components retain the normal distribution.

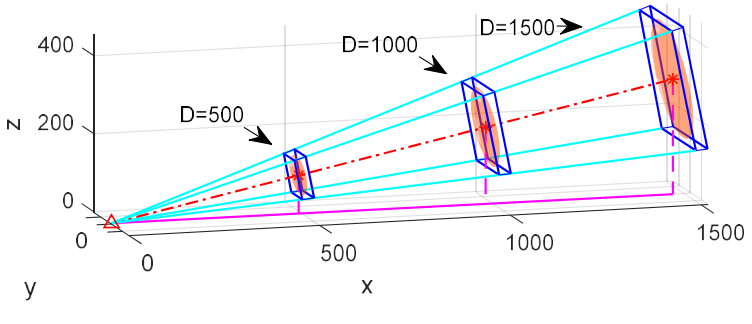

Fig. 2. Layout of optoelectronic stations, AC, actual and Chebyshev forms and boundaries of uncertainty regions of AC location during open observation of OES

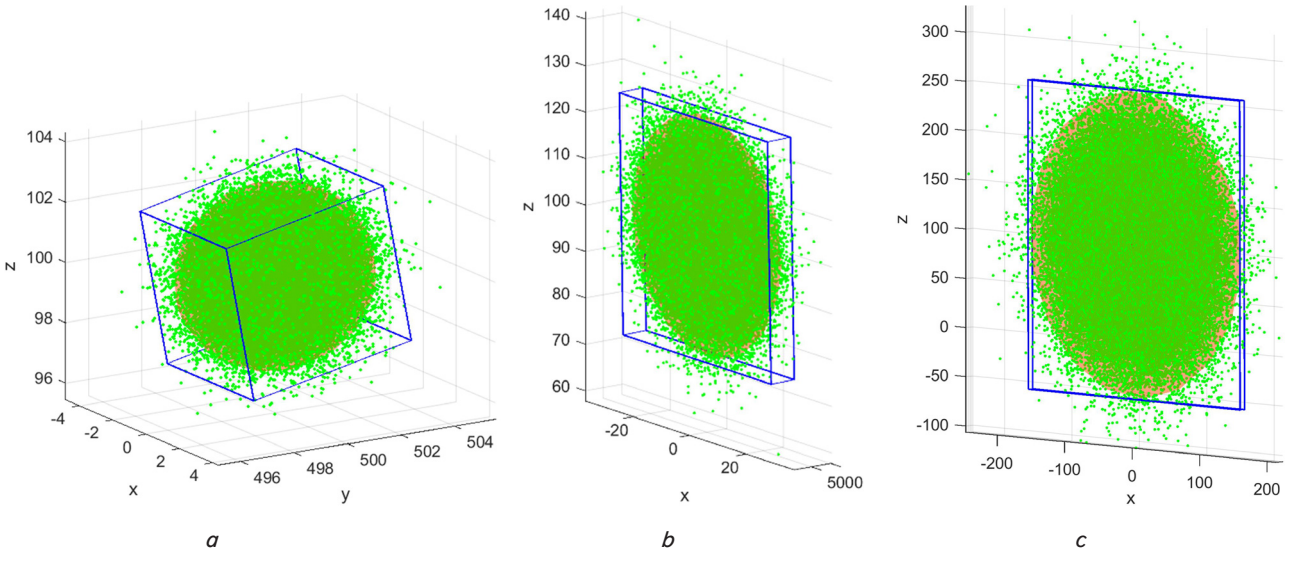

Fig. 3. Actual values of AC position (green dots) and (blue) Chebyshev forms and boundaries of the uncertainty regions of AC position for open observation by one optoelectronic station from a distance to the AC: *a* – 500 m; *b* – 5 km; *c* – 30 km

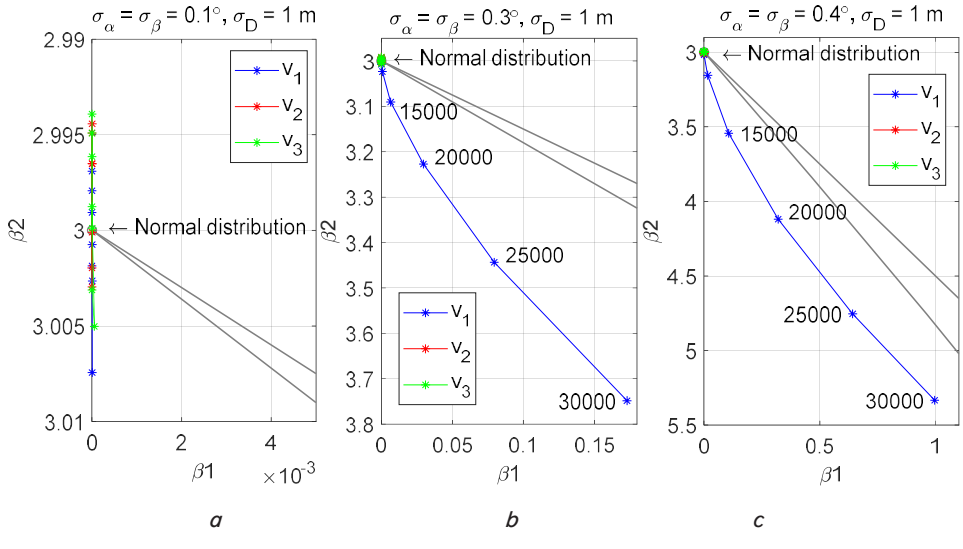

Fig. 4. Values of estimates β_1, β_2 for each component of AC location error vector during open observation by one optoelectronic station with the value $\sigma_\alpha = \sigma_\beta$: *a* – 0.1°; *b* – 0.3°; *c* – 0.4°

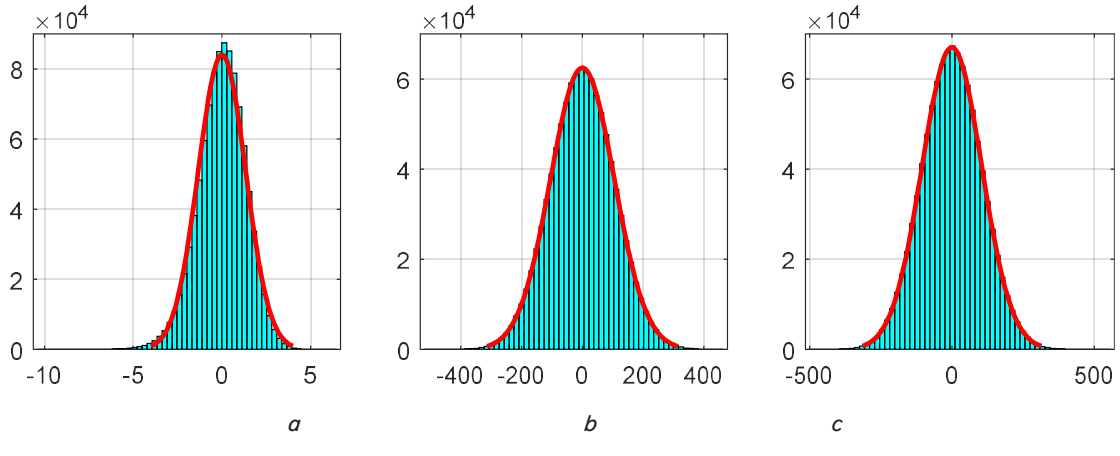

Fig. 5. Histograms of the distribution of AC location errors for a distance of 15 km and $\sigma_\alpha = \sigma_\beta = 0.4°$ for each coordinate **v**: *a* – v_1; *b* – v_2; *c* – v_3

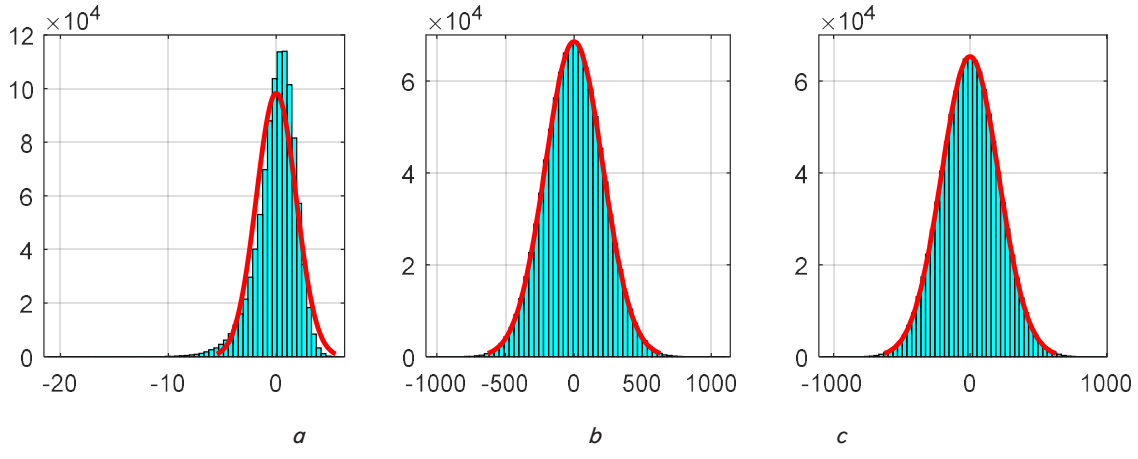

Fig. 6. Histograms of the distribution of AC location errors for a distance of 30 km and $\sigma_\alpha = \sigma_\beta = 0.4°$ for each coordinate **v**: *a* – $\mathbf{v}_1$; *b* – $\mathbf{v}_2$; *c* – $\mathbf{v}_3$

5. 5. 2. Observation by two optoelectronic stations

When simulating observation by two OESs, the distance between them was taken to be 1000 m (fixing the observation base). The location of AC was chosen symmetrically with respect to the OES at the same distance from each. The distance to the AC was chosen to provide a given angle (γ) between the lines of sight from the OES to the AC. The MSD of OES geopositioning was taken to be 0.5 m, i.e., $\sigma_{X_i} = \sigma_{Y_i} = \sigma_{Z_i} = 0.5$ m. The MSD of errors in the direct measurements of azimuth, elevation angle, and inclined range were taken to be $\sigma_\alpha = 0.1°$, $\sigma_\beta = 0.1°$, $\sigma_D = 1$ m.

5. 5. 3. Open observation by two optoelectronic stations

Fig. 7 shows the layout of OES, AC, actual and Chebyshev forms and boundaries of the uncertainty regions of AC location with increased measurement errors $\sigma_{X_i} = \sigma_{Y_i} = \sigma_{Z_i} = 1$ m, $\sigma_\alpha = \sigma_\beta = 2°$, $\sigma_D = 5$ m, and a distance to the AC of 500 m for clarity. For this modeling scenario, a significant spread of MSD was obtained along each of the coordinates $\sigma_1 = 6.9953$, $\sigma_2 = 7.8984$, $\sigma_3 = 9.2873$.

Fig. 8 shows the shapes and boundaries of the uncertainty region for open observation by two OESs with angles between the lines of sight of 70.53° and 3.82°.

Fig. 9, 10 show histograms of the distribution of AC location errors for each of the components of AC location coordinate vector from a distance of $D = 866$ m with angles between the lines of sight $\gamma = 70.53°$ and $D = 15017$ m at $\gamma = 3.82°$.

Fig. 14 shows values of estimates β_1, β_2 for each of the coordinates of the vector $\boldsymbol{\nu}$ of AC location errors for open 14*a*, and covert 14*b*, observation by two OESs for the base between OES 1000 m with a distance $D = 866$ m at an angle between the lines of sight $\gamma = 70.53°$. Analysis of the results shown in Fig. 9, 10, 14 allows us to conclude that increasing the distance from OES to AC does not violate the symmetry of the law of error distribution but leads to an increase in kurtosis, i.e., to a deviation of the law of error distribution of AC location coordinates from normal towards the Student's *t*-distribution.

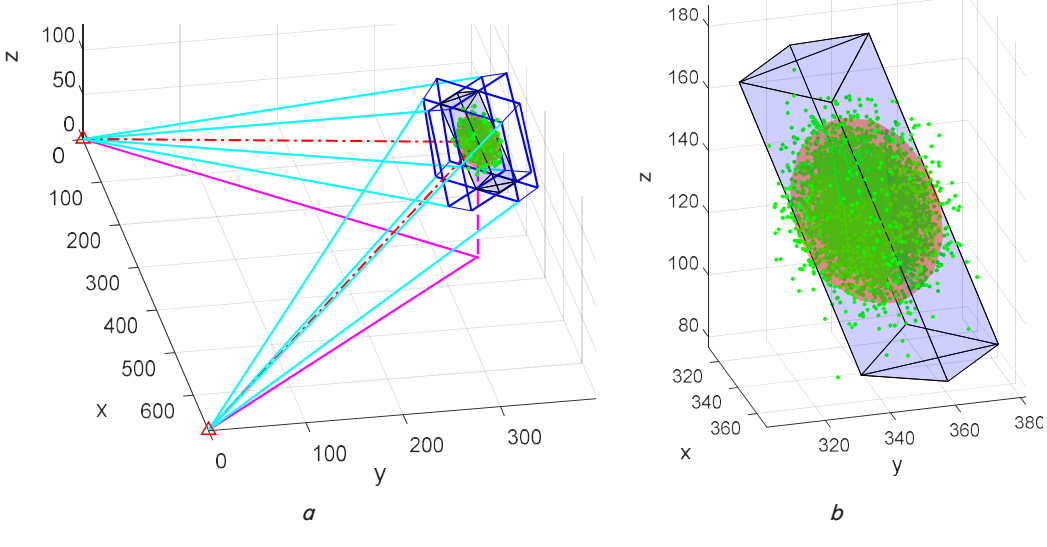

Fig. 7. Layout of optoelectronic stations, AC, actual and Chebyshev forms and boundaries of uncertainty regions of AC location with increased measurement errors: *a* – layout; *b* – separate uncertainty region

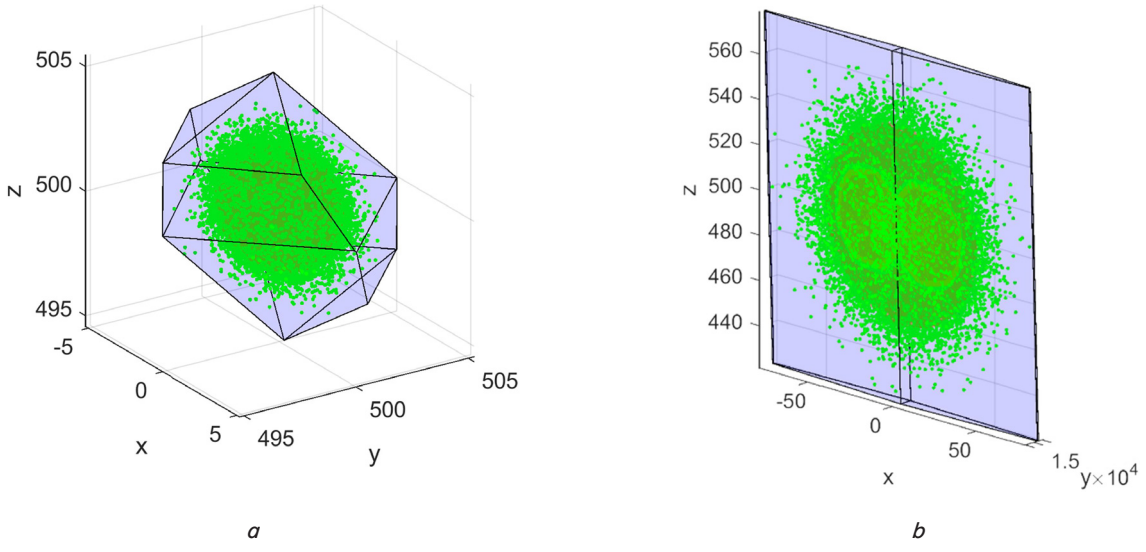

a *b*

Fig. 8. Shapes and boundaries of the uncertainty region for open observation by two optoelectronic stations with angles between the lines of sight: *a* – γ = 70.53°; *b* – γ = 3.82°

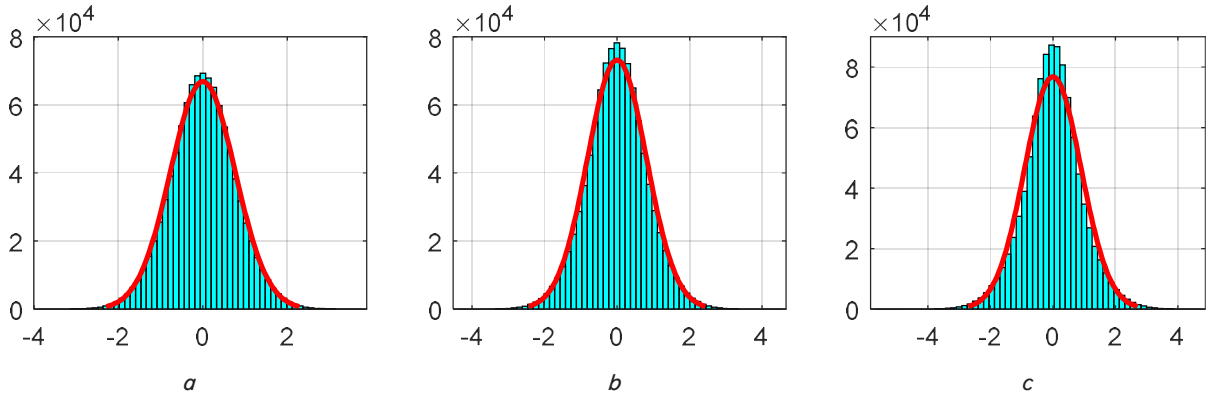

a *b* *c*

Fig. 9. Histograms of the distribution of AC location errors for a distance D = 866 m at γ = 70.53° for each coordinate **v**: *a* – v_1; *b* – v_2; *c* – v_3

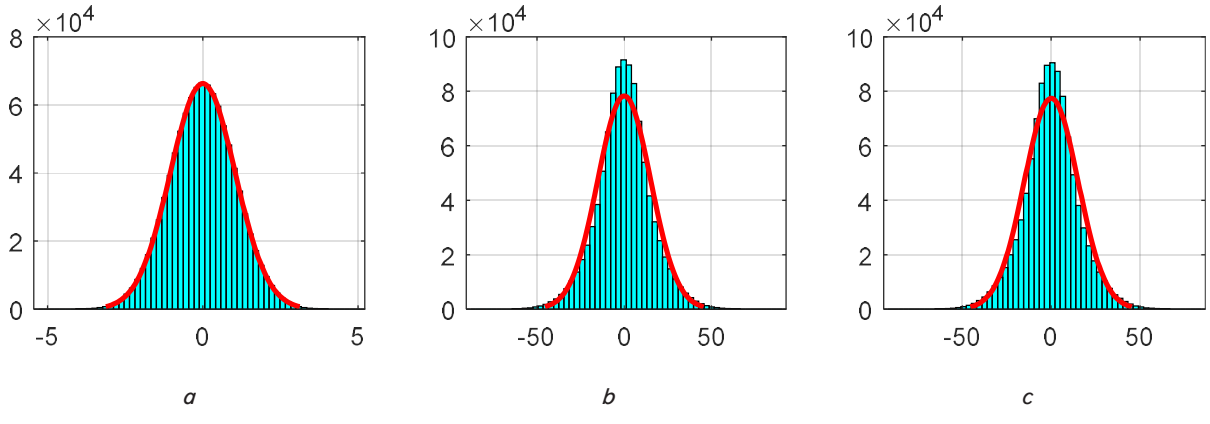

a *b* *c*

Fig. 10. Histograms of the distribution of AC location errors for a distance D = 15017 m at γ = 3.82° for each coordinate **v**: *a* – v_1; *b* – v_2; *c* – v_3

5. 5. 4. Covert observation by two optoelectronic stations

For a comparative analysis of open and covert observation, simulation modeling of covert observation by two stations was carried out similarly to open observation.

Analysis of the results shown in Fig. 12, 13 allows us to conclude that the laws of distribution of AC location errors for each of the components **v** of AC location coordinate vector practically do not differ from the normal one.

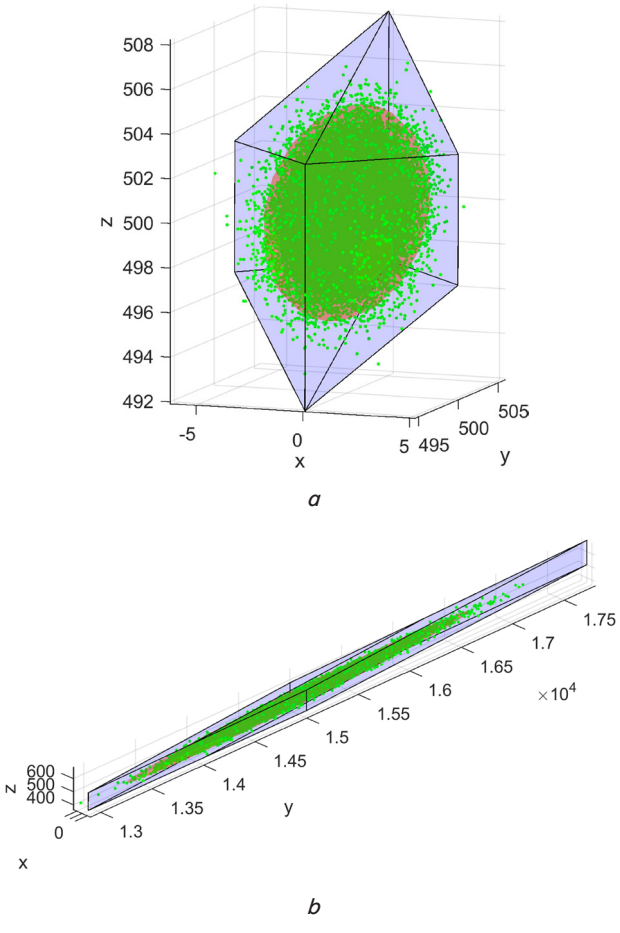

Fig. 11. Shapes and boundaries of the uncertainty region for covert surveillance by two optoelectronic stations with angles between the lines of sight: *a* – $\gamma = 70.53°$; *b* – $\gamma = 3.82°$

5. 5. 5. Comparison of open and covert observation by two optoelectronic stations

Fig. 14 shows the values of estimates β_1, β_2 for each of the coordinates $\mathbf{v} = (v_1, v_2, v_3)$ of AC location error vector for open (*a*) and covert (*b*) observation by two OESs for a base of 1000 m. Table 1 gives results of the comparative analysis for open and covert observation for two OES configurations.

Table 1

Results of comparative analysis for two types of observation

Type	Open	Covert
$\gamma = 70.53°$, $D = 866$ m		
σ	(0.90, 0.81, 0.76)	(1.73, 1.22, 1.06)
β_1	(0, 0, 0)	(0, 0, 0)
β_2	(3.74, 3.41, 3.26)	(3.0, 3.0, 3.0)
$\gamma = 3.82°$, $D = 15017$ m		
σ	(15.13, 15.12, 1.04)	(558.01, 18.57, 18.55)
β_1	(0, 0, 0)	(0.047, 0, 0)
β_2	(3.86, 3.85, 3.02)	(3.09, 3.02, 3.02)
Δ	(0, 0, 0)	(0.0315, 0.6425, 0.0276)

During open observation by two OESs, the distribution of values of the vector $\mathbf{v} = (v_1, v_2, v_3)$ of AC location errors along each of the coordinates v_1 and v_2 has the character of a Student's *t*-distribution. Coordinate v_3 has a normal distribution, and with increasing distance and decreasing angle γ it approaches the Student's *t*-distribution (Fig. 14). During covert observation, coordinates v_2, v_3 have a distribution close to normal, which with increasing distance to the AC shifts to the Student's *t*-distribution. Coordinate v_1 has a distribution close to normal and with decreasing angle γ it changes to the Johnson distribution S_U (Fig. 14, *b*).

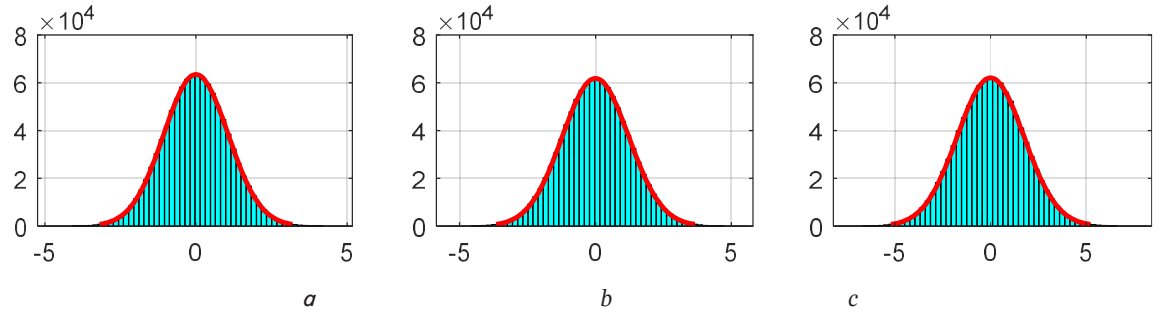

Fig. 12. Histograms of the distribution of AC location errors for a distance of $D = 866$ m at $\gamma = 70.53°$ for each coordinate **v**: *a* – v_1; *b* – v_2; *c* – v_3

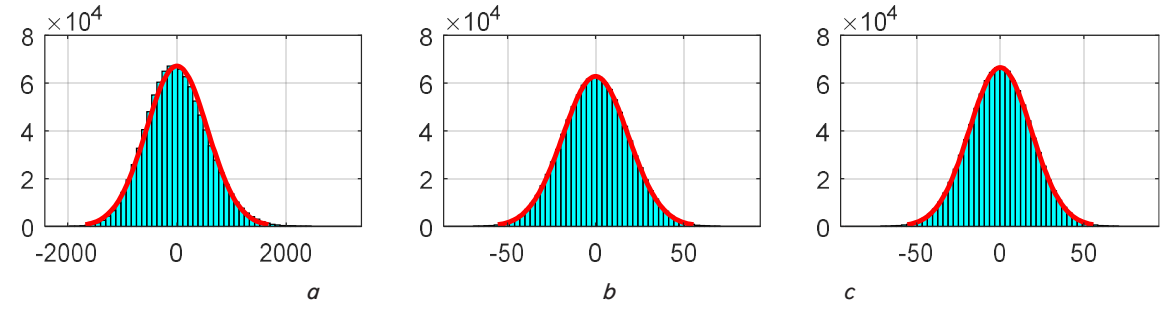

Fig. 13. Histograms of the distribution of AC location errors for a distance $D = 15017$ m at $\gamma = 3.82°$ for each coordinate **v**: *a* – v_1; *b* – v_2; *c* – v_3

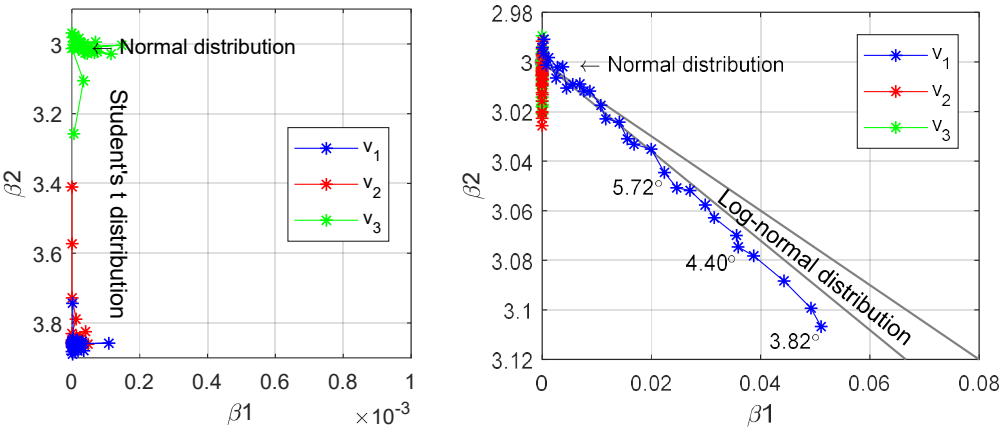

Fig. 14. Values of estimates β_1, β_2 for observation by two optoelectronic stations with a base between them of 1000 m: *a* – open; *b* – covert

5. 5. 6. Covert observation by two optoelectronic stations at small angles γ between the lines of sight

Fig. 15 shows the values of estimates β_1, β_2 for coordinates **v** for three values of angle $\gamma = 1°, 2°, 3°$ between the lines of sight of OES on AC. During covert observation, the distortion of the shape of the uncertainty zone sharply increases with a decrease in the angle γ between the lines of sight. A simulation of covert observation by two stations with small angles between the lines of sight for different distances to AC was carried out.

Analysis of the results shown in Fig. 15 reveals that during covert observation, the distortion of the uncertainty zone depends on the angle between the lines of sight and the errors in measuring the direction to AC but depends little on the distance to the AC. The deviation from the normal distribution law is shown in Fig. 16, 17 relative to the red line.

Table 2 gives the results of modeling covert surveillance for AC at a distance of 1000 m and $\gamma = 1°, 2°$.

Analysis of the results given in Table 2 reveals that when observing at small angles between the lines of sight, the mathematical expectation (center of the scattering ellipsoid) is shifted from the real position of AC.

Table 2

Results of covert observation simulation for $\gamma = 1°, 2°$

γ	1°	2°
σ	(154.43, 1.30, 1.26)	(74.69, 1.29, 1.25)
β_1	(0.87,0, 0)	(0.17, 0, 0)
β_2	(3.91, 3.28, 3.27)	(3.36, 3.06, 3.04)
Δ	(–0.3326, –1.2414, –0.0003)	(–0.0843, –0.3156, –0.0003)

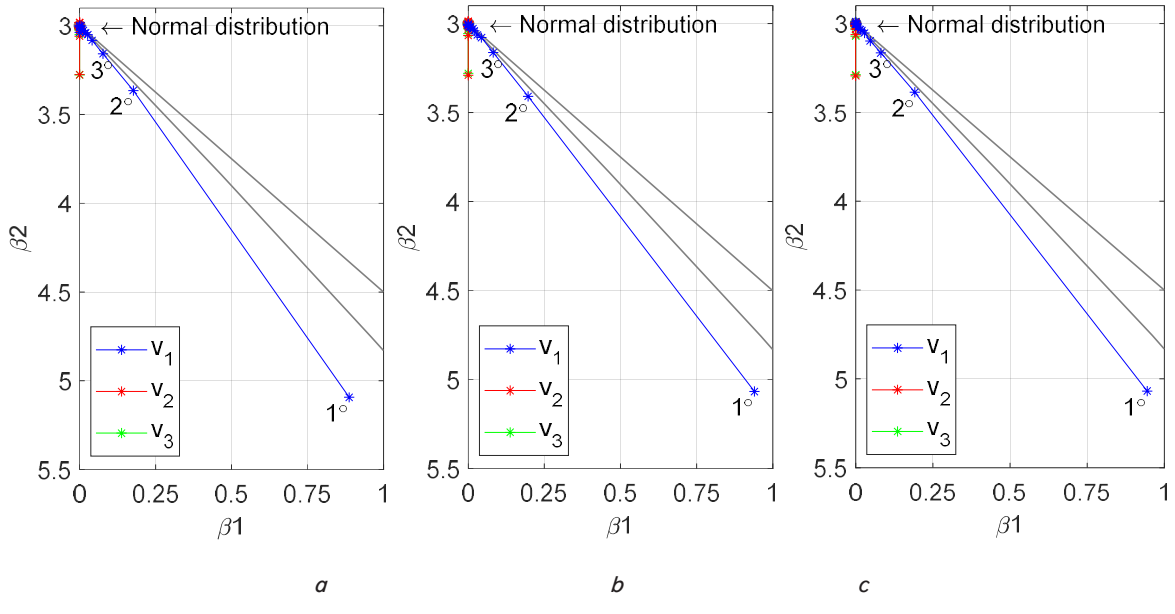

Fig. 15. Values of estimates β_1, β_2 for covert surveillance by two optoelectronic stations at $\gamma = 1°, 2°, 3°$ for distances: *a* – 1000 m; *b* – 25000 m; *c* – 50000 m

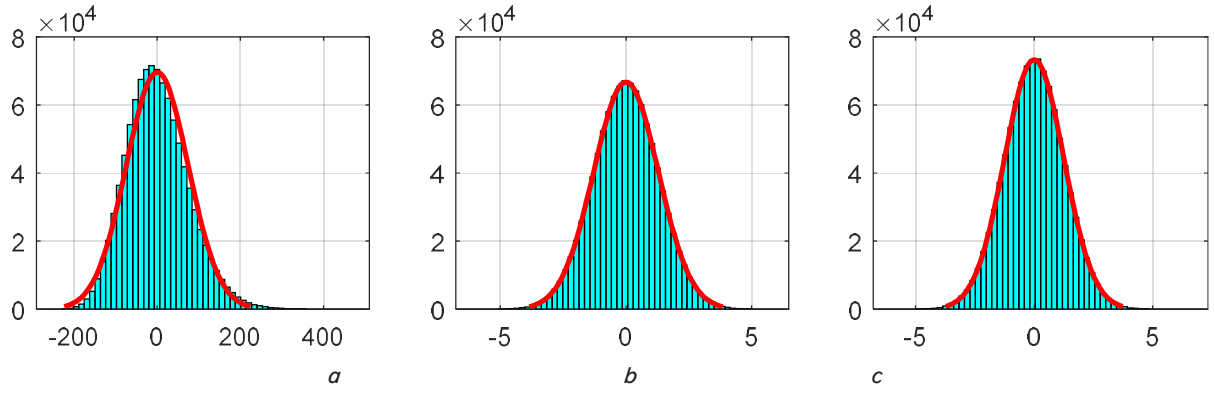

Fig. 16. Histograms of the distribution of AC location errors for a distance $D = 1000$ m at $\gamma = 2°$ along each coordinate **v**: $a - v_1$; $b - v_2$; $c - v_3$

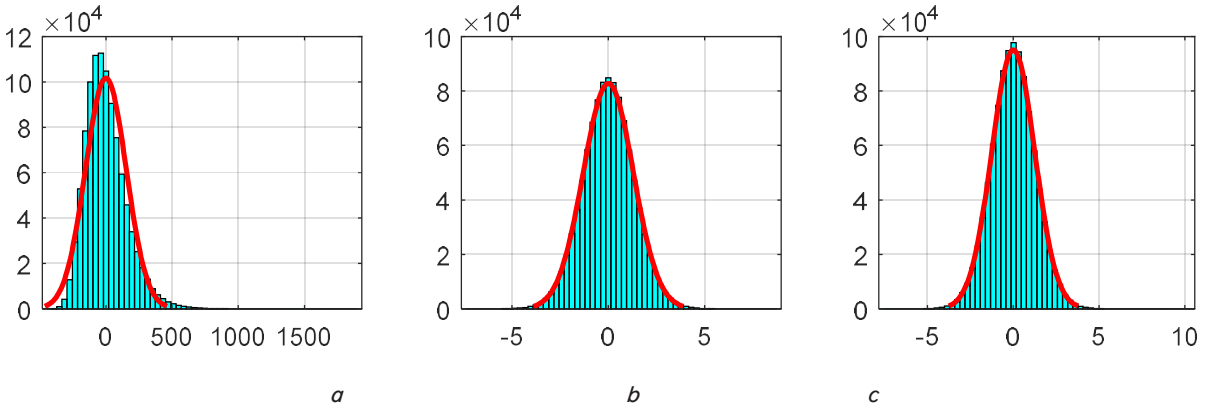

Fig. 17. Histograms of the distribution of AC location errors for a distance $D = 1000$ m at $\gamma = 1°$ for each coordinate **v**: $a - v_1$; $b - v_2$; $c - v_3$

5. 5. 7. Comparison of open and covert observation by three optoelectronic stations

Simulation of open and covert observation by three OESs was carried out for an AC located at a distance of 1225 m from all OESs (Fig. 18).

Fig. 19 shows the shapes and boundaries of the uncertainty region for open (Fig. 19, *a*) and hidden (Fig. 19, *b*) observation by three OESs. Histograms of the distribution of errors in AC location for each component of the vector of coordinates of AC location and the results of their approximation by a normal distribution for open observation by three OESs are shown in Fig. 20, for hidden observation in Fig. 21. According to the results of modeling open observation, σ (0.93, 0.81, 0.76), β_1 (0, 0, 0), β_2 (3.88, 3.46, 3.31). The values of β_1, β_2 correspond to the Student's *t*-distribution.

The simulation of covert observation by three OESs was carried out similarly to open observation. Unlike open observation, covert observation (not at acute angles γ) does not distort the uncertainty zone and can be fully described by a scattering ellipsoid at σ (1.85, 1.53, 1.25), β_1 (0, 0, 0), β_2 (3.0, 3.0, 3.0).

Similarly to observation by two OESs, with open observation by three OESs, the laws of error distribution for each of the coordinates of vector **v** remain symmetric, and the kurtosis increases to the Student's *t*-distribution, and with covert observation, the normal distribution is preserved for all coordinates.

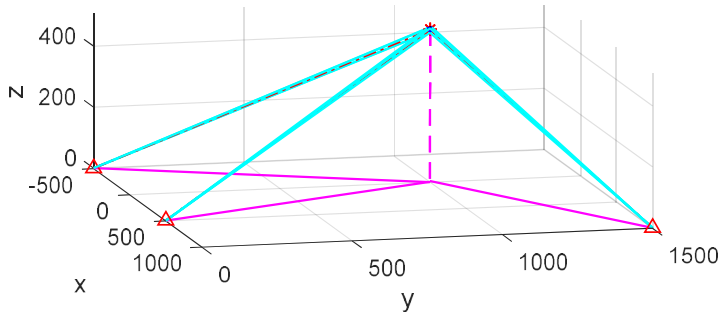

Fig. 18. Layout of optoelectronic stations and AC for observation by three stations

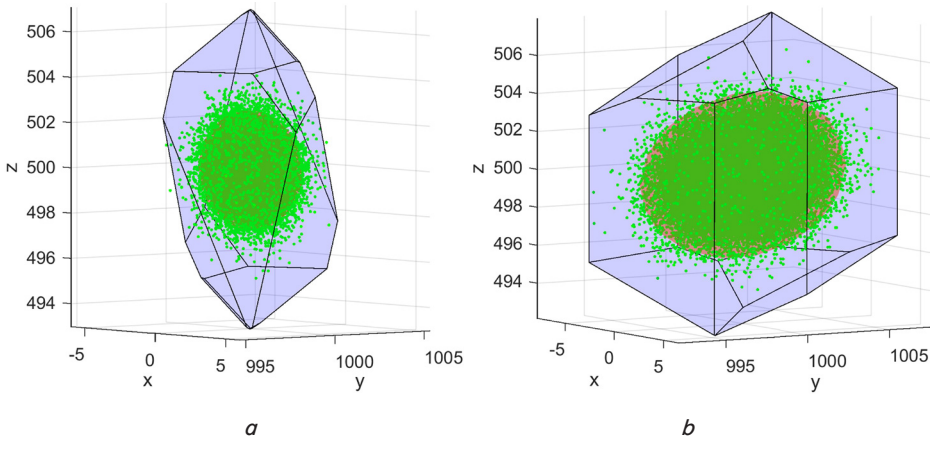

Fig. 19. Shapes and boundaries of the uncertainty region for observation by three optoelectronic stations: *a* — open; *b* — covert

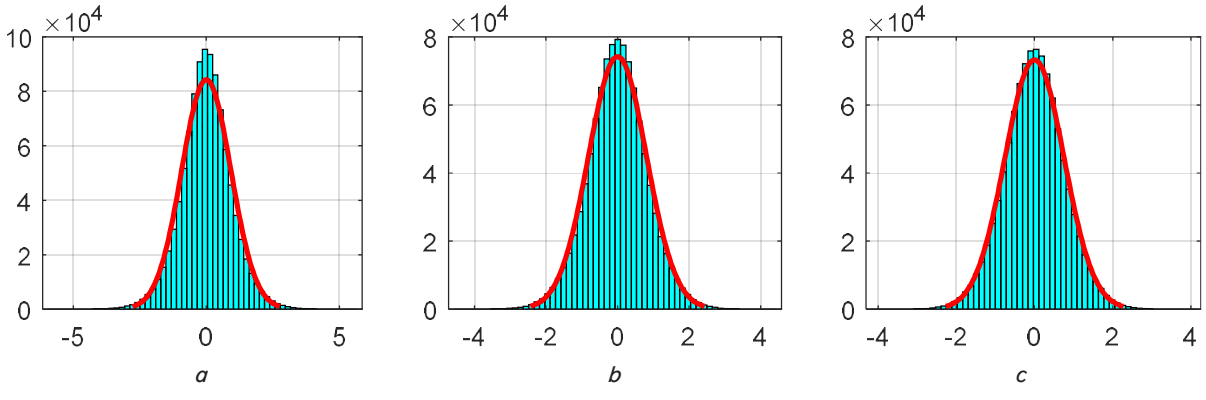

Fig. 20. Histograms of the distribution of errors in the location of AC for open observation by three optoelectronic stations for each coordinate **v**: *a* — v_1; *b* — v_2; *c* — v_3

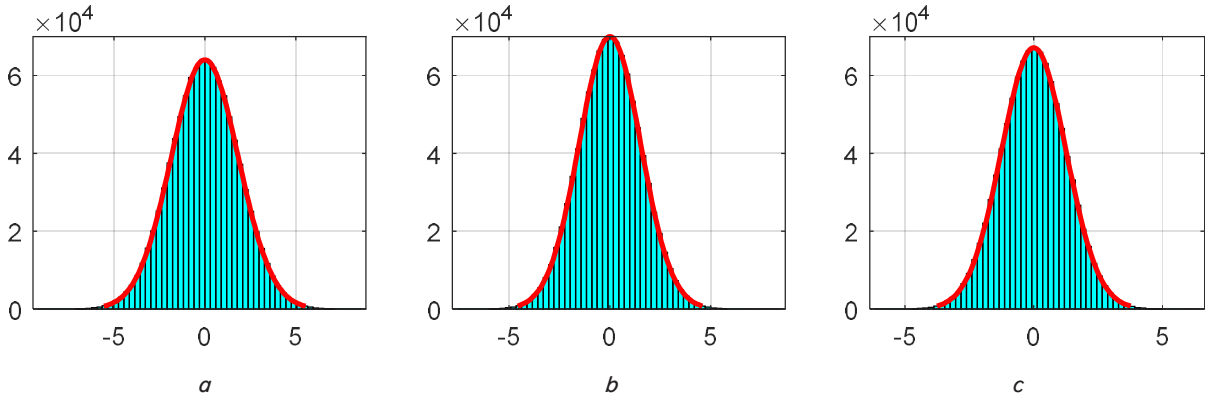

Fig. 21. Histograms of the distribution of errors in the location of an AC for covert surveillance by three optoelectronic stations for each coordinate **v**: *a* — v_1; *b* — v_2; *c* — v_3

6. Discussion of results based on assessing the accuracy of AC positioning

The presence of errors in the results of video surveillance of OES ICN for AC leads to the fact that instead of estimating the exact location of the AC in the airspace, it is possible to estimate only the boundaries of the uncertainty region (47), (48) in which, with a given probability, the AC is located. Practically in all modern studies, the scattering ellipsoid [16, 20–22] is used as an estimate of the accuracy of AC location, which corresponds to the hypothesis of the normality of the distribution of errors in AC location estimates.

The theoretical basis for using this hypothesis is the laws of large numbers (LNL) and the central limit theorem (CLT). LNL does not take into account the distribution shapes of random variables, and CLT establishes the conditions under which the distribution of random variables tends to normal. Thus, a necessary and sufficient condition for its use is the assumption of normality of the distribution of errors in the estimates of the location of AC. The question about what to do if this condition is not met remained open. Unlike [16, 20–22]

and many others, in which the scattering ellipsoid is used, our work shows that the shape of this region is a convex polyhedron. For a comparative analysis of the proposed method (convex polyhedron) with the classical method (scattering ellipsoid), we have devised and investigated a numerical method for assessing the accuracy of AC positioning using the ICN of OES by simulating the processes of open and covert video surveillance. The simulation modeling was carried out under the assumption that all video surveillance errors are distributed according to a normal law with the corresponding MSD values.

The results allowed us to evaluate the statistical properties of the errors in AC location estimates under different observation conditions and confirm that the assumption of normality of the distribution of these errors is not always valid. The paper proposes a numerical method for assessing the accuracy of AC positioning in the form of a convex polyhedron for the case when the assumption of normality of the distribution of AC location estimates errors is not met.

Based on the results of our research, simulation models of the processes of open and covert observation of AC by the ICN of OES were built, which make it possible to take into account errors in geopositioning and measurement of azimuth and elevation angle, changing the distance to the observation object and the spatial location of OES. This provided the possibility of a comprehensive analysis of the influence of various factors on the accuracy of AC positioning.

An algorithm for numerically estimating errors in AC location coordinates based on the results of OES observation has been developed. The algorithm takes into account different types of observation (open and covert), variations in errors in direct measurements, and the geometry of the observation base. This has made it possible to calculate position error vectors and analyze their statistical properties in a wide range of scenarios.

Based on the results of simulation modeling, it was established that with high accuracy of direct measurements, coordinate errors are approximated by a normal distribution (Fig. 4). With increasing measurement errors or under the condition of open observation, deviations of the error distribution towards the Student's t-distribution or the Johnson distribution S_U occur (Fig. 5, 6). It was found that covert observation is characterized by a more stable behavior of errors with predominantly normal distributions (Table 1).

A method has been devised for constructing a universal estimate of the accuracy of AC positioning in the form of a convex polyhedron (47), (48), in which the AC is located with a given probability. The shape and boundaries of the convex polyhedron depend on the numerical value of the parameter k and a priori information about the statistical properties of the errors in the estimates of AC location coordinates. If the density functions of the distribution of RVs of the video surveillance results are unknown, and only their first two moments are known – the mathematical expectation and the variance, then at $k = 3$ the lower bound of the probability that the AC is located inside the uncertainty sector takes the value $P \geq 0.88889$. If it is additionally known that the density function of the distribution of RVs is symmetric with respect to its mathematical expectation, the lower probability limit increases to $P \geq 0.9506$. For a normal distribution, the lower probability limit is $P \geq 0.9973$.

A comparative analysis of error distributions during open and covert observation with two (Fig. 11) and three OESs (Fig. 18) was conducted. Open observation is accompanied by the appearance of distributions with increased kurtosis (Student's t-distribution) (Fig. 9, 10, 14), which indicates an increase in the probability of small errors. Covert observation is characterized by a closer to normal distribution of errors for all coordinates, which provides higher predictability of positioning accuracy.

In the case of open observation with two OESs, the law of error distribution for each of the coordinates of the vector $\mathbf{v}$ takes the form of a Student's t-distribution, the kurtosis of which increases with increasing distance and decreasing angle γ between the lines of sight (Fig. 15). In this case, it is also advisable to use a convex polyhedron as an estimate of the accuracy of AC positioning.

In covert observation by two OESs at a viewing angle of $\gamma > 30°$, the distribution of errors along each of the coordinates of vector $\mathbf{v}$ remains normal. In the case of a decrease of $\gamma < 30°$, only coordinate v_1 demonstrates a shift to the Johnson distribution S_U (Fig. 16, 17). The distributions of errors along coordinates v_2 and v_3 remain close to normal even when the distance to the object changes. Thus, covert observation is characterized by more stable statistical properties of the errors of the coordinates of vector $\mathbf{v}$ compared to the open one, which makes it possible to describe the uncertainty region using the SE at $\gamma > 30°$. For acute angles γ, it is more efficient to use a convex polyhedron.

In the case of covert observation at $\gamma \leq 3°$, as a result of systematic errors in the estimates of the mathematical expectation of the components of vector $\mathbf{v}$, the asymmetry of the error distribution along the coordinate v_1 increases sharply, a "heavy tail" of the convex polyhedron appears and SE goes beyond its boundaries (Table 2). This practically does not depend on the distance to AC. Such an observation mode is impractical due to the obtained shift in the estimates of AC coordinates.

The results of the observation simulation by three OESs confirmed the trends identified for two OESs: for open observation, the distribution of errors with a larger kurtosis (approaching the Student's t-distribution) is characteristic (Fig. 20), while with covert observation the distribution remained close to normal along all coordinates (Fig. 21).

The method devised for assessing the accuracy of AC positioning in the form of a convex polyhedron allows us to obtain the exact boundaries of the uncertainty region in which, with a given probability, the AC is located for any unimodal law of error distribution of AC location estimates in airspace. This becomes possible due to the fact that for any law of the distribution of SV with known parameters, there are standard procedures for calculating the boundaries in which SV is located with a given probability. For covert video surveillance, this region is a tetrahedral pyramid with the vertex at the point of the location of OES. The height of such a pyramid is determined by the direct visibility range of OES. For open video surveillance, this region is a truncated pyramid, the height of which is determined by the law of distribution of the error in measuring the inclined range to AC, the estimate of its MSD and the probability that the true value of the inclined range to AC will be within this height. The angles between the faces of the pyramid are determined by the laws of distribution of the error of measurements of azimuth and elevation angle of OES, numerical values of MSD and the probability that the true values of azimuth and elevation angle will be within the limits between the corresponding faces of the pyramid. If video surveillance of AC is carried out simultaneously by n OES ICN, then the shape and boundaries of the error region of the video surveillance results are determined by the inner region of convex polyhedra (47) for open surveillance and (48) for covert surveillance. These general results are valid for any unimodal laws of distribution of errors of estimates of the location of AC in the airspace.

The method is limited in that it makes it possible to obtain the exact boundaries of the uncertainty region provided that the parameters and the law of distribution of random errors of AC location estimates for standard video surveillance conditions are precisely known. Under actual conditions, the influence of external influences can significantly change the statistical properties of video surveillance errors and their significant difference from known ones, which can lead to a change in the numerical value of the probability of finding the AC inside a convex polyhedron.

Regarding the possible shortcomings of the method, the following can be noted. The studies were conducted under a static mode, in which the coordinates of OES geopositioning and the location of AC in the airspace were accurately a priori known. This allowed us to accurately calculate the azimuth, elevation angle, and slope range, on which, according to the simulation models, normally distributed errors were superimposed. Under actual conditions, at best, only some estimates of these coordinates are known, and the construction of estimates of the accuracy of AC positioning is carried out in real time for each moment of video surveillance. This leads to the need to consider the results of simulation modeling as a reference.

This study in the future may focus on a more detailed determination of the dependence of the actual probability value that the AC is indeed located within the Chebyshev uncertainty region – a convex polyhedron, on the specific values of parameters for various distribution laws, in particular the Student's t-statistics and Johnson distribution S_U. Knowledge of this dependence would allow us to minimize the dimensions of the convex polyhedron for a given probability value and will provide the possibility of using the Chebyshev uncertainty region as a universal measure of assessing the accuracy of AC positioning in airspace.

7. Conclusions

1. The problem of assessing the accuracy of AC positioning by OES ICS is quite complex, and its solution depends on many factors: the distribution laws and numerical values of the parameters of random errors of the geopositioning estimates of OES and direct measurements of the azimuth, elevation angle, and inclined range from each i-th OES to AC; the mutual spatial location of OES and AC (the distance between the OES and the AC and the angle γ between the lines of sight of OES to AC); the video surveillance modes of AC (open/covert); the number of OESs that simultaneously conduct video surveillance of AC, and others.

2. The assumption that for a normal law of distribution of errors of the results of direct video observations of OES ICN of AC, the law of distribution of errors of AC location along each of the coordinates will also be normal is far from always valid. This is most clearly manifested as a result of nonlinear transformations of random errors of the results of direct video observations in the event of an increase in their MSD > 0.1° and an increase in the bias of mathematical expectation estimates with a decrease in $\gamma < 30°$ in the algorithm for estimating errors of AC location coordinates.

3. At small values of MSD of direct measurement errors (less than 0.1°) and a change in the values of angles between the lines of sight from $\gamma = 120°$ to $\gamma = 30°$, the law of distribution of AC location errors along each of the coordinates of AC location error vector $\mathbf{v} = (v_1, v_2, v_3)$ regardless of the modes of video surveillance of AC by OES ICN (open/covert) remains normal. The scattering ellipsoid could be used as a measure of AC positioning accuracy.

4. At $\gamma < 30°$, nonlinear transformations lead to significant changes in the law of distribution of AC location errors, which can be approximated by the Johnson distribution S_U, and it is advisable to use a convex polyhedron as a measure of AC positioning accuracy.

5. If the distribution laws of errors in estimates of AC location coordinates differ from the normal one in at least one of the coordinates, then it is advisable to use a convex polyhedron as a measure of the AC positioning accuracy.

Conflicts of interest

The authors declare that they have no conflicts of interest in relation to the current study, including financial, personal, authorship, or any other, that could affect the study, as well as the results reported in this paper.

Funding

The source of funding for manufacturing a prototype of OES for the detection and tracking of moving objects in the air environment is the Scientific and Technical Research Project "Development of technology for high-precision guidance of means of defeating air objects" under the contract dated 09.03.2021 No. DZ/105–2021 and the Scientific and Technical Research Project "Development of technology for the detection and high-precision tracking of air objects" under the contract dated 05.11.2018 No. DZ/60-2018.

Data availability

All data are available, either in numerical or graphical form, in the main text of the manuscript.

Use of artificial intelligence

The authors confirm that they did not use artificial intelligence technologies when creating the current work.

Acknowledgments

The authors express their gratitude to the team at the research plant of the Kharkiv National University of Radio Electronics, and personally to engineers A.Cherkashin, M. Yeletin, and V. Krylov.

References

1. Bensky, A. (2016). Wireless Positioning Technologies and Applications. Artech House, 424.
2. Lazzari, F., Buffi, A., Nepa, P., Lazzari, S. (2017). Numerical Investigation of an UWB Localization Technique for Unmanned Aerial Vehicles in Outdoor Scenarios. IEEE Sensors Journal, 17 (9), 2896–2903. https://doi.org/10.1109/jsen.2017.2684817

3. Semenyuk, V., Kurmashev, I., Lupidi, A., Alyoshin, D., Kurmasheva, L., Cantelli-Forti, A. (2025). Advances in UAV detection: integrating multi-sensor systems and AI for enhanced accuracy and efficiency. International Journal of Critical Infrastructure Protection, 49, 100744. https://doi.org/10.1016/j.ijcip.2025.100744
4. Saadaoui, F. Z., Cheggaga, N., Djabri, N. E. H. (2023). Multi-sensory system for UAVs detection using Bayesian inference. Applied Intelligence, 53 (24), 29818–29844. https://doi.org/10.1007/s10489-023-05027-z
5. Stuckey, H., Escamilla, L., Garcia Carrillo, L. R., Tang, W. (2024). Real-Time Optical Localization and Tracking of UAV Using Ellipse Detection. IEEE Embedded Systems Letters, 16 (1), 1–4. https://doi.org/10.1109/les.2023.3234871
6. Stuckey, H., Al-Radaideh, A., Escamilla, L., Sun, L., Carrillo, L. G., Tang, W. (2021). An Optical Spatial Localization System for Tracking Unmanned Aerial Vehicles Using a Single Dynamic Vision Sensor. 2021 IEEE/RSJ International Conference on Intelligent Robots and Systems (IROS), 3093–3100. https://doi.org/10.1109/iros51168.2021.9636665
7. Golyak, I. S., Anfimov, D. R., Golyak, I. S., Morozov, A. N., Tabalina, A. S., Fufurin, I. L. (2020). Methods for real-time optical location and tracking of unmanned aerial vehicles using digital neural networks. Automatic Target Recognition XXX, 50. https://doi.org/10.1117/12.2573209
8. Nam, S. Y., Joshi, G. P. (2017). Unmanned aerial vehicle localization using distributed sensors. International Journal of Distributed Sensor Networks, 13 (9), 155014771773292. https://doi.org/10.1177/1550147717732920
9. Hu, F., Wu, G. (2020). Distributed Error Correction of EKF Algorithm in Multi-Sensor Fusion Localization Model. IEEE Access, 8, 93211–93218. https://doi.org/10.1109/access.2020.2995170
10. Sorbelli, F. B., Pinotti, C. M., Silvestri, S., Das, S. K. (2022). Measurement Errors in Range-Based Localization Algorithms for UAVs: Analysis and Experimentation. IEEE Transactions on Mobile Computing, 21 (4), 1291–1304. https://doi.org/10.1109/tmc.2020.3020584
11. Vitiello, F., Causa, F., Opromolla, R., Fasano, G. (2024). Radar/visual fusion with fuse-before-track strategy for low altitude non-cooperative sense and avoid. Aerospace Science and Technology, 146, 108946. https://doi.org/10.1016/j.ast.2024.108946
12. Bala, A., Muqaibel, A. H., Iqbal, N., Masood, M., Oliva, D., Abdullahi, M. (2025). Machine learning for drone detection from images: A review of techniques and challenges. Neurocomputing, 635, 129823. https://doi.org/10.1016/j.neucom.2025.129823
13. Yan, X., Fu, T., Lin, H., Xuan, F., Huang, Y., Cao, Y. et al. (2023). UAV Detection and Tracking in Urban Environments Using Passive Sensors: A Survey. Applied Sciences, 13 (20), 11320. https://doi.org/10.3390/app132011320
14. Svanstrom, F., Englund, C., Alonso-Fernandez, F. (2021). Real-Time Drone Detection and Tracking With Visible, Thermal and Acoustic Sensors. 2020 25th International Conference on Pattern Recognition (ICPR), 7265–7272. https://doi.org/10.1109/icpr48806.2021.9413241
15. Tevyashev, A., Zemlyaniy, O., Shostko, I., Kostaryev, D., Paramonov, A. (2024). Devising an analytical method for estimating aircraft positioning accuracy by an infocommunication network of optoelectronic stations. Eastern-European Journal of Enterprise Technologies, 5 (9 (131)), 36–48. https://doi.org/10.15587/1729-4061.2024.312762
16. Zekavat, S. A. (Reza), Buehrer, R. M. (Eds.) (2011). Handbook of Position Location. Wiley. https://doi.org/10.1002/9781118104750
17. Khudov, H., Berezhnyi, A., Oleksenko, O., Maliuha, V., Balyk, I., Herda, M., Sobora, A. et al. (2023). Increasing of the accuracy of determining the coordinates of an aerial object in the two-position network of small-sized radars. Eastern-European Journal of Enterprise Technologies, 5 (9 (125)), 6–13. https://doi.org/10.15587/1729-4061.2023.289623
18. Zheng, Q., Chen, J., Yang, R., Shan, Z. (2017). Research on airborne infrared location technology based on orthogonal multi-station angle measurement method. Infrared Physics & Technology, 86, 202–206. https://doi.org/10.1016/j.infrared.2017.08.019
19. Putyatin, V. G., Dodonov, A. G. (2017). Ob odnoy zadache vysokotochnyh traektornyh izmereniy opticheskimi sredstvami. Reiestratsiya, zberihannia i obrobka danykh, 19 (2), 36–54. Available at: http://nbuv.gov.ua/UJRN/rzod_2017_19_2_6
20. Dodonov, A. G., Putyatin, V. G. (2017). Nazemnye opticheskie, optiko-elektronnye i lazerno-televizionnye sredstva traektornyh izmereniy. Matematychni mashyny i systemy, 4, 30–56. Available at: http://dspace.nbuv.gov.ua/bitstream/handle/123456789/131985/02-Dodonov.pdf?sequence=1
21. Tevjashev, A., Zemlyaniy, O., Shostko, I., Paramonov, A. (2024). Mathematical Models and Methods of Observation and High-Precision Assessment of the Trajectories Parameters of Aircraft Movement in the Infocommunication Network of Optoelectronic Stations. 2nd International Congress of Electrical and Computer Engineering, 295–309. https://doi.org/10.1007/978-3-031-52760-9_21
22. Shostko, I., Tevyashev, A., Zemlyaniy, O., Tsibulnikov, D. (2023). Designing and testing a prototype of optical-electronic station for detecting and tracking moving objects in the air. Eastern-European Journal of Enterprise Technologies, 6 (5 (126)), 36–42. https://doi.org/10.15587/1729-4061.2023.295101
23. Hofmann-Wellenhof, B., Lichtenegger, H., Collins, J. (2001). Global Positioning System. Springer Vienna. https://doi.org/10.1007/978-3-7091-6199-9
24. Hahn, G. J., Shapiro, S. S. (1994). Statistical models in engineering. Wiley, 376.
25. Precise Simulation. GEOMLib version 1.0. GitHub. Available at: https://github.com/precise-simulation/geomlib/releases/tag/1.0